Incorporating elastic and creep deformations in modelling the three-dimensional autogenous shrinkage of cement paste

Gao, Peng; Ye, Guang; Huang, Haoliang; Qian, Zhiwei; Schlangen, Erik; Wei, Jiangxiong; Yu, Qijun

DOI
10.1016/j.cemconres.2022.106907

Publication date
2022

Document Version
Final published version

Published in
Cement and Concrete Research

Citation (APA)
Gao, P., Ye, G., Huang, H., Qian, Z., Schlangen, E., Wei, J., & Yu, Q. (2022). Incorporating elastic and creep deformations in modelling the three-dimensional autogenous shrinkage of cement paste. *Cement and Concrete Research*, *160*, Article 106907. https://doi.org/10.1016/j.cemconres.2022.106907

Cement and Concrete Research 160 (2022) 106907

Contents lists available at ScienceDirect

Cement and Concrete Research

journal homepage: www.elsevier.com/locate/cemconres

Incorporating elastic and creep deformations in modelling the three-dimensional autogenous shrinkage of cement paste

Peng Gao [a,b], Guang Ye [c], Haoliang Huang [b,d], Zhiwei Qian [e], Erik Schlangen [c], Jiangxiong Wei [b,d,*], Qijun Yu [a,b,d,*]

[a] School of Civil Engineering, Hefei University of Technology, Hefei 230009, China
[b] School of Materials Science and Engineering, South China University of Technology, 510640 Guangzhou, China
[c] Microlab, Faculty of Civil Engineering and Geosciences, Delft University of Technology, 2628, CN, Delft, the Netherlands
[d] Guangdong Low Carbon Technologies Engineering Centre for Building Materials, 510640 Guangzhou, China
[e] FEMRIS, The Hague 2497, CJ, the Netherlands

ARTICLE INFO

Keywords:
Autogenous shrinkage
Three-dimensional
Effective stress
Effective modulus
Lattice fracture model

ABSTRACT

A structure-based modelling framework was established to simulate the three-dimensional autogenous shrinkage of cement paste. A cement hydration model, HYMOSTRUC3D-E, was used to obtain the microstructures and ionic concentrations of the cement paste. A lattice fracture model based on the effective stress and effective modulus was used to consider the elastic and creep parts of autogenous shrinkage. For Portland cement pastes with water-to-cement ratios of 0.3 and 0.4 (where the time zero of autogenous shrinkage was set as the time of the drop in internal relative humidity), the simulated linear elastic autogenous shrinkage was respectively −188 and −79 μm/m at 160 h. The obtained linear total autogenous shrinkage including elastic and creep deformations was respectively −501 and −236 μm/m at 160 h. These values of the elastic autogenous shrinkage and total autogenous shrinkage are close to the predications of poromechanical models and experimental data obtained using a corrugated tube.

1. Introduction

Autogenous shrinkage is a main reason for the cracking of high-performance concrete; indeed, the autogenous shrinkage of high-performance concrete is often appreciable at an early age owing to a low water-to-cement (W/C) ratio (e.g., <0.4) and a high content of pozzolans, such as silica fume [1,2]. There is considerable interest in predicting the autogenous shrinkage of cement paste [3–8] because it is important for the optimization of binders with less autogenous shrinkage and can be used to evaluate the autogenous shrinkage of concrete [9,10].

Cement paste is a porous material that comprises a solid skeleton, capillary pores, and gel pores. In modelling the autogenous shrinkage of cement paste, a central problem is to consider the imposing of the driving force on the solid skeleton of the cement paste. In recent decades, poromechanical models have attracted much attention [3,6–8]. In developing the poromechanical models, the change in the pore fluid pressure, such as the capillary pressure, has been considered as the force driving shrinkage. The concept of effective stress has been adopted to establish the linear relationship between the autogenous shrinkage and driving force, wherein the effective stress has been calculated as a function of the degree of saturation of the cement paste, the driving force and bulk modulus of the cement paste and the bulk modulus of the solid skeleton of the cement paste [3]. Lura et al. [3], for example, considered the cement paste as elastic material and calculated the autogenous shrinkage of the cement paste using poromechanical models. They found that the simulated autogenous shrinkage of cement paste was much smaller than the experimental result with the progression of the decrease in relative humidity (RH). This difference between simulation and experiment was probably due to the time-dependent behaviour of the cement paste (i.e., creep) not being included in the poromechanical models [3,6–8]. The quantification of the creep part of autogenous shrinkage has thus become an important research topic in recent years [6–8,11,12]. Hu et al. [6], for example, used the Kelvin-Voigt model to predict the visco-elastic component of cement paste. Lu et al. [7] calculated the creep part of autogenous shrinkage as a function of the activation energy of cement paste. The obtained autogenous shrinkage was in line with experimental observations.

* Corresponding authors at: School of Materials Science and Engineering, South China University of Technology, 510640 Guangzhou, China.
E-mail addresses: jxwei@scut.edu.cn (J. Wei), concyuq@scut.edu.cn (Q. Yu).

https://doi.org/10.1016/j.cemconres.2022.106907
Received 25 October 2021; Received in revised form 4 July 2022; Accepted 9 July 2022
Available online 31 July 2022

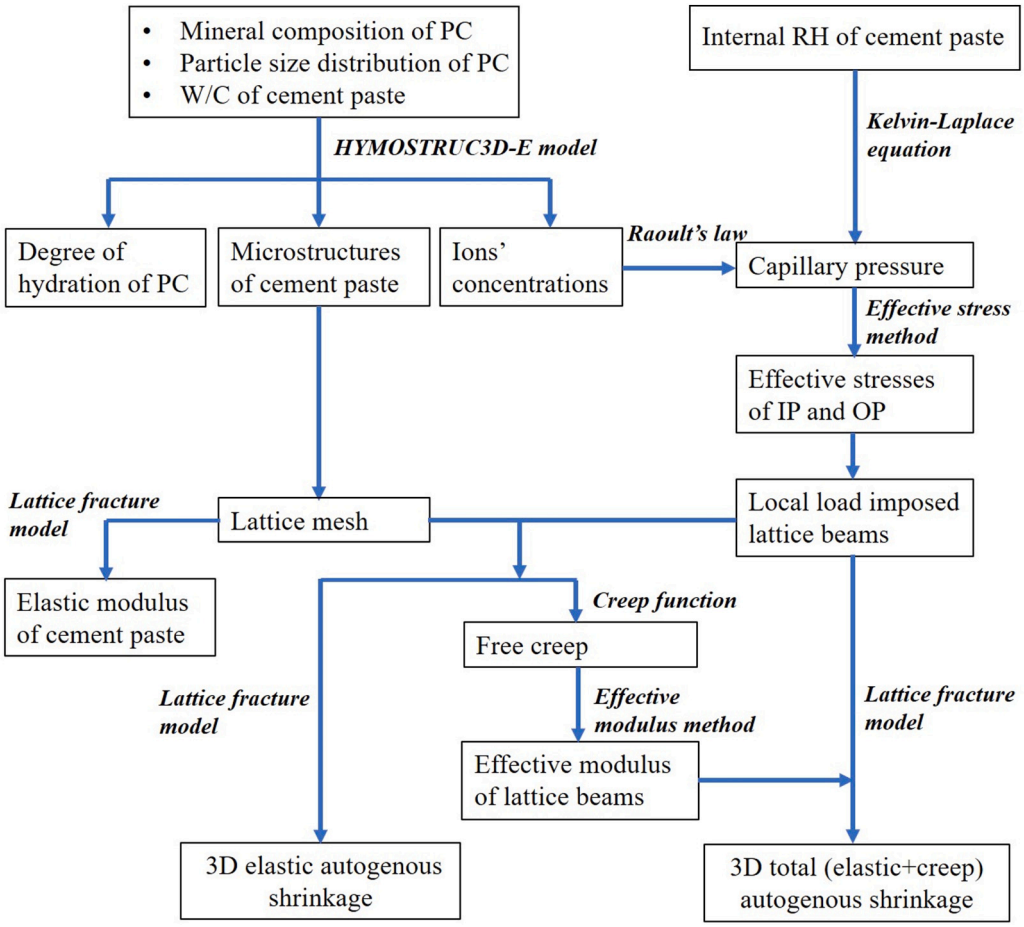

Fig. 1. Schematic diagram for simulating the 3D autogenous shrinkage of cement paste.

As computer science and technology have advanced, modellers have directly quantified and visualised the three-dimensional (3D) microscale deformations of porous materials. Bentz et al. [13], for example, used a finite element method to impose the capillary force on the pore wall of porous Vycor in simulating the elastic deformations of porous Vycor glass. In a recent study by our group [5], the microstructure of cement paste was established using a cement hydration model (HYMOSTRUC3D). The 3D autogenous shrinkage of cement paste was obtained by applying the lattice fracture model to impose capillary pressure on the capillary water-solid surface of cement paste. Additionally, Liu et al. [14] used the lattice fracture model to simulate the 3D drying shrinkage of cement paste, wherein the capillary pressure was imposed on C-S-H gels and the capillary water-solid surface of cement paste. However, these studies did not quantify the creep part of shrinkage in the 3D modelling process. Do et al. [8] recently applied a finite element method to obtain the creep compliance of cement paste by considering the local creep compliance of the hydration products of cement. The obtained creep properties of cement paste were then applied in poromechanical models to quantify the contribution of creep in the autogenous shrinkage of cement paste [8]. These studies suggest that the autogenous shrinkage of cement paste can be simulated using a 3D modelling method such as the finite element method. However, there remains the need to incorporate both the elastic and creep deformations in modelling the 3D autogenous shrinkage of cement paste.

The current study established a structure-based modelling framework to address both the elastic part and creep part of the autogenous shrinkage of cement paste. The elastic part was obtained by applying the lattice fracture model in simulating the imposing of a local force on the hydration products of cement at the microscale. The shrinkage of hydration products, which was calculated by applying the poromechanical model, was used to calculate the local force imposing on the hydration products. The creep compliance of hydration products, which was calculated following the creep function by considering the hydration time of cement, was used to calculate the effective modulus of hydration products. By applying the lattice fracture model, the obtained effective modulus was used to address the 3D autogenous shrinkage of cement paste involving both the elastic part and creep part.

2. Modelling methods

Fig. 1 shows the modelling methods used in this study. The study models (1) the hydration, microstructures and ionic concentrations of the cement paste; (2) the 3D elastic autogenous shrinkage of the cement paste; (3) the 3D total autogenous shrinkage of the cement paste; and (4) the Young's modulus of the cement paste. The microstructures of cement pastes, which were obtained using the cement and hydration model, were different in different simulations because the particles were randomly packed in the cube. This might affect the simulation results of autogenous shrinkage. To consider this influence, simulations were conducted three times for each of (1) to (4).

2.1. Hydration, microstructures and ionic concentrations of the cement paste

The HYMOSTRUC3D-E model was used to obtain the hydration, microstructures and ionic concentrations of the cement paste. The HYMOSTRUC3D-E model was developed by the Delft University of Technology to handle the hydration and microstructure of Portland

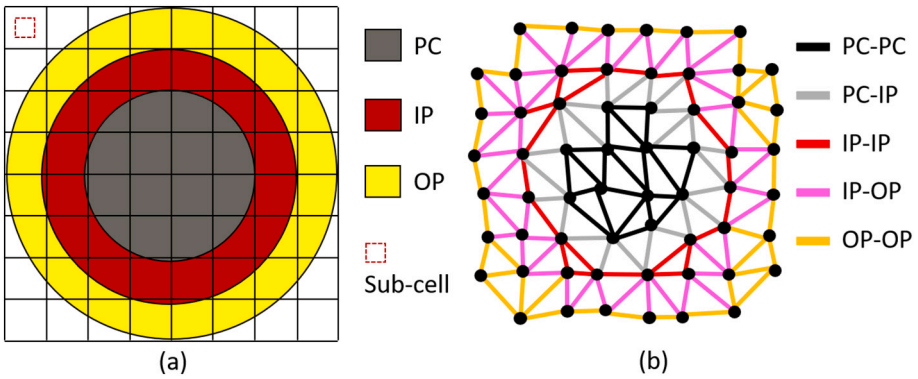

Fig. 2. Schematic diagram for establishing the lattice mesh from the microstructure of the cement paste output by the HYMOSTRUC3D-E model. Note that PC-OP elements are not shown in this figure. However, it is possible to have PC-OP elements with two digitising adjacent particles.

cement (PC) paste blended with blast furnace slag and/or fly ash [15,16]. The main inputs of the HYMOSTRUC3D-E model were the mineral composition and particle size distribution of the cement and the W/C ratio of the cement paste. A hydration module was established to calculate the reaction rates of the cement as a function of the water distribution, ionic concentrations, and temperature of the system. A pore solution module, which was based on Taylor's method [17] and the solubility equilibria of calcium hydroxide and gypsum, was used to simulate the ionic concentrations. A cement particle growth module was used to deal with the penetration of cement particles and the precipitation of inner and outer hydration products. The representative elementary volume of the cement paste was set at $100 \times 100 \times 100\ \mu m^3$. A discrete logarithmic time was used in the simulation (see Fig. A.1). Further details of the HYMOSTRUC3D-E model are presented in Appendix A.

2.2. Three-dimensional elastic autogenous shrinkage of the cement paste

The progression of the hydration process decreases the RH of the sealed cement paste and thereby affects the internal stresses and leads to the autogenous shrinkage of cement paste [1–3]. In principle, the driving forces of autogenous shrinkage such as capillary forces are imposed on the solid surfaces that are wetted by water. Many researchers used the poromechanical models to describe this process and predict the linear autogenous shrinkage of cement paste [6–8]. At the microscale, the solid skeleton of the cement paste comprises unreacted PC, inner hydration products (IPs) and outer hydration products (OPs). IPs and OPs are porous phases that have smaller capillary pores and gel pores. With ongoing hydration of cement, unreacted PC are surrounded by IPs and OPs. To simulate the 3D autogenous shrinkage of cement paste at the microscale, it is necessary to consider how to impose the driving forces of autogenous shrinkage at this scale.

In current study, the capillary forces are assumed to be imposed on the solid surfaces that are wetted by water in the porous IPs and OPs, and cause the shrinkage of IPs and OPs. As the internal RH decreases, the IPs and OPs shrink, which cause the generation of local forces at the microscale. The local forces will result in the deformation of cement paste. In the simulation, the key point is how to calculate the local forces imposed on the IPs and OPs. The current study utilized the poromechanical models to predict the autogenous shrinkage of the per unit volumes of IPs and OPs, and used a concept of effective forces to calculate the local forces imposed on the IPs and OPs. After that, the 3D elastic autogenous shrinkage was simulated using a lattice fracture model to impose the local forces on all the IPs and OPs of cement paste. In comparison with the traditional poromechanical models, the advantage of the current study is to simulate how the autogenous shrinkage of IPs and OPs cause the 3D autogenous shrinkage of cement paste at the microscale.

In a lattice fracture model, discretised lattice elements are often used to describe the structure of an object. The non-linear behaviour of materials is analysed in a sequence of linear analysis steps. In each step, the lattice analysis is similar to the standard finite element analysis [18–20]. Generally, the lattice fracture model has the advantage of computing efficiency [18–20]. In recent years, the lattice fracture model has been applied in many studies to deal with the fracture behaviours of cement-based materials [14,18–23]. The current study used a lattice fracture modelling program (GLAK) established by the Delft University of Technology. The details of the modelling process are presented as follows.

(1) Lattice mesh

The lattice mesh of the cement paste was constructed using the method of Qian et al. [18–20]. The mesh size is an important parameter in the lattice modelling, because it will impact the simulated fracture behaviour of cement-based materials. Normally, the local mechanical properties of cement particles should be considered by setting a proper mesh size. According to the study of Qian et al. [18–20], a mesh with resolution of $2 \times 2 \times 2\ \mu m^3$/cell was used to digitise the microstructure of the cement paste output by the HYMOSTRUC3D-E model (as shown in Fig. 2a). A sub-cell ($1 \times 1\ \mu m^2$) was placed in each cell. Lattice nodes were randomly generated on the sub-cells and designated as PC, IP and OP according to the main phase in the cell. A triangulation mesh can be used to simulate the deformations (e.g., drying-induced deformations) of cement-based materials in lattice fracture modelling [24], and the lattice elements were thus obtained by connecting the lattice nodes following the Delaunay triangulation algorithm [24,25] (Fig. 2b). Depending on the types of connected lattice node, the lattice elements are denoted PC-PC, IP-IP and OP-OP and the interface elements are denoted PC-IP, PC-OP and IP-OP.

(2) Mechanical properties of lattice elements

Qian et al. [19,20] recently established a multiscale framework for simulating the fracture behaviour of cement-based materials using the lattice fracture model. They also obtained PC-PC, IP-IP, OP-OP, PC-IP, PC-OP and IP-OP lattice elements by connecting lattice nodes. The mechanical properties of PC-PC, IP-IP and OP-OP were taken from the literature. The Young's modulus and shear modulus of interface elements were calculated from the mechanical properties of connected phases using the harmonic average. The compressive strength and tensile strength of interface elements were respectively set as the lower value of the compressive strength and tensile strength of the connected phases. Liu et al. [14] applied this method to calculate the mechanical properties of lattice elements in modelling the drying shrinkage of cement paste. The method of Qian et al. [20] was used in the current

Table 1
Mechanical properties of lattice elements [20].

	Young's modulus (GPa)	Shear modulus (GPa)	Compressive strength (GPa)	Tensile strength (GPa)
PC-PC	135	52	18	1.8
IP-IP	30	12	2.4	0.24
OP-OP	22	8.9	1.5	0.15
PC-IP	49	20	2.4	0.24
IP-OP	25	10	1.5	0.15
PC-OP	38	15	1.5	0.15

study. Table 1 gives the obtained mechanical properties of lattice elements.

(3) Local force imposed on the lattice mesh

The effective stress method was used to calculate the local force imposed on the lattice mesh. The effective stress is defined as the internal stress exerted by the pore water on the solid phase [7,26]. Many studies have used the effective stress method to calculate the linear shrinkage of cement-based materials [3,6,7]. IPs and OPs are porous phases that contain pore water and it was thus assumed that capillary pressure can be imposed on the solid phase of IPs and OPs via the pore water, causing the linear shrinkage of IPs and OPs. To calculate the effective stress of IPs and OPs, it is necessary to quantify the pore structures of IP and OPs. However, the quantification of the pore structures of IPs and OPs is a challenging issue. Different researchers obtained different pore structures of IP and OPs. For the convenience of comparison, the current study used the Jennings colloid model of C-S-H gel [27] to describe the pore structures of IPs and OPs. The effective stresses of IP and OP phases were calculated using the bulk moduli of IPs, OPs and C-S-H globules and the capillary pressure based on the effective stress concept (see Eq. (1)).

$$\sigma_{eff,i} = \left(1 - \frac{K_i}{K_{glo}}\right) S_w \sigma_{cap} \tag{1}$$

Here, K_i is the bulk modulus of IPs or OPs and K_{glo} is the bulk modulus of C-S-H globules. S_w is the degree of saturation of IPs or OPs. σ_{cap} is the capillary pressure. The pore size of IPs or OPs is in the nanoscale range (e.g., <5 nm) and the internal RH of sealed cement paste is normally higher than 80 %. According to the Kelvin and Laplace equations, the empty pore size is larger than 10 nm in diameter, which exceeds the pore size of IPs or OPs. S_w was thus set as 1 in the current study. Notably, the S_w might be changed if the pore structures of IPs and OPs are quantified in further experiments or models.

The bulk modulus of IPs or OPs was calculated from the Young's modulus and Poisson ratio of the IPs or OPs (Eq. (2)). In reality, the Poisson ratios of hydration products, such as C-S-H gel, are time dependent [28]. Hu et al. [6] used an empirical function to describe the time-dependent behaviour of the Poisson ratio of cement paste. However, the function for describing the evolution of the Poisson ratios of hydration products is unclear, particularly at an early age. In the current study, the Poisson ratios of IPs and OPs were set constant (0.24) according to Do et al. [8]. The same method was used to calculate the bulk modulus of C-S-H globules, wherein the Young's modulus of C-S-H globules was set at 47.75 GPa according to the literature [14]. The capillary pressure was calculated using the Kelvin-Cohan equation by considering the effect of ions on RH [6] (Eq. (3)).

$$K_i = \frac{E_i}{3(1 - 2\upsilon_i)} \tag{2}$$

Here, E_i is the Young's modulus of IPs or OPs, and υ_i is the Poisson ratio of IPs or OPs.

$$\sigma_{cap} = -\frac{RT ln\left(\frac{RH}{RH_S}\right)}{V_m} \tag{3}$$

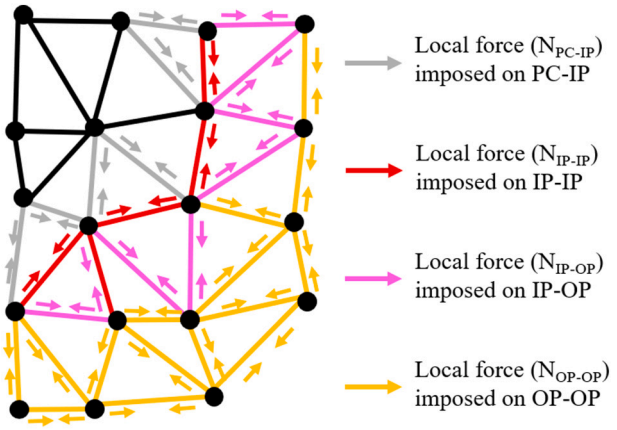

Fig. 3. Schematic diagram of imposing local forces on lattice elements.

Here, RH is the measured internal RH of the cement paste and RH_S is the RH reduction factor calculated from the ionic concentrations of the cement paste (Eq. 4). V_m is the molar volume of capillary water, R is the molar gas constant (8.314 $Jmol^{-1}$ L^{-1}), and T is the temperature (K).

$$RH_s = \frac{n_{wat}}{n_{wat} + c_{Na^+} + c_{K^+} + c_{Ca^{2+}} + c_{SO_4^{2-}} + c_{OH^-}} \tag{4}$$

Here, n_{wat} is the amount of capillary water. c_{Na^+}, c_{K^+}, $c_{Ca^{2+}}$, $c_{SO_4^{2-}}$ and c_{OH^-} are the ionic concentrations in the capillary water simulated using the HYMOSTRUC3D-E model. Notably, the influence of ions on the RH can be quantified more accurately by considering the ionic strength of pore solution [29].

The effective forces imposed on IP-IP and OP-OP lattice elements were calculated using Eq. (5). The effective forces imposed on PC-IP and PC-OP lattice elements were set as the same as those imposed on IP-IP and OP-OP lattice elements, respectively. The effective force imposed on IP-OP lattice elements was set as the average of the effective forces imposed on PC-IP and PC-OP lattice elements.

$$N_i = \sigma_{eff,i} A \tag{5}$$

Here, N_i is the effective force imposed on IP-IP or OP-OP lattice elements. A is the cross-sectional area of lattice elements. A was calculated from the radius of lattice elements following the method of Qian et al. [18–20].

To simulate the elastic autogenous shrinkage of the cement paste, local forces were imposed on the lattice elements using the lattice modelling software GLAK [18–20] (Fig.3). In the modelling process of GLAK, the local forces (N_i) were reduced as initial forces ($N_{i,\ ini}$) and imposed on IP-IP, OP-OP, PC-IP, PC-OP and IP-OP lattice elements. Tensile stresses were exerted in some elements owing to the restraining of PC-PC elements. GLAK searched for the element with the highest ratio of tensile stress to tensile strength. GLAK then strengthened the local forces ($N_{i,\ bro}$) until this element was broken. In the current study, this process proceeded only one step because N_i were smaller than $N_{i,\ bro}$. GLAK then output the coordinates of lattice nodes and the residual stresses of lattice elements. The coordinates of lattice nodes and the

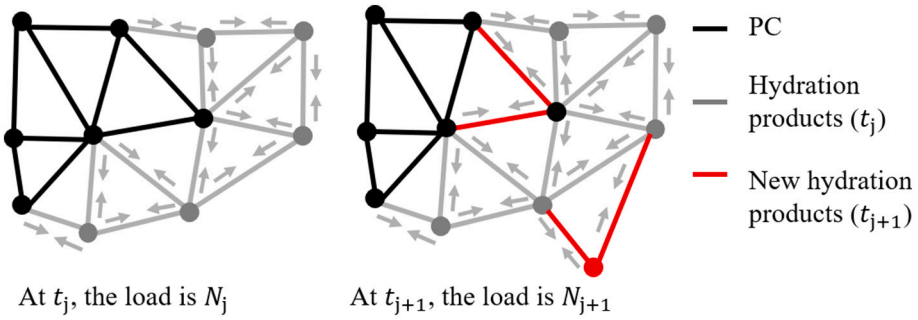

Fig. 4. Schematic diagram of considering the effects of the incremental load and new hydration products on the stress redistribution of the system.

residual stresses of lattice elements were adjusted depending on the ratio of $N_{i,\,bro}$ to N_i. By using the above simulation process, the elastic internal restraint shrinkage of cement paste was obtained. The linear elastic autogenous shrinkage of the cement paste ($\varepsilon_{lin,\,ela}$) was calculated as the average deformations of the nodes on surfaces divided by the size of the cement paste.

The microstructure of cement paste changes with the ongoing hydration of cement. Additionally, the local forces change. It is important to consider these dynamic changes in modelling the autogenous shrinkage of cement paste. As schematically shown in Fig. 4, as the time changes from t_j to t_{j+1}, new hydration products form in the system and change the force equilibrium of the previous step, which will redistribute the stress of the system formed at the previous hydration time. Furthermore, the load changes from N_j to N_{j+1}. The incremental load (N_{j+1}-N_j) also changes the stress in the system. In considering these two aspects, we used the lattice model to impose the load N_{j+1} on the new structure including the added hydration products. In this way, the effects of both the incremental load (N_{j+1}-N_j) and the added hydration products on the stress redistribution of the system were considered.

2.3. Three-dimensional total autogenous shrinkage of the cement paste

Imposing effective stress will result in creep in the IP-IP, OP-OP, PC-IP, PC-OP and IP-OP lattice elements. In the present study, this creep is called free creep. The total free shrinkage is the sum of the free elastic shrinkage and free creep. However, due to the restraining of other lattice elements such as PC-PC, the total free shrinkage of lattice elements will be affected. The corresponding shrinkage is called the total internal restraint shrinkage. To simulate the 3D elastic and creep shrinkage, we calculated the total free shrinkage of lattice elements based on creep functions and simulated the internal restraint shrinkage by incorporating the effective modulus concept in the lattice fracture model. The simulation process is presented as follows.

(1) Total free shrinkage of lattice elements

The free creep of lattice elements was calculated from the creep compliance (J) and the differentials of effective stress ($\Delta\sigma_{eff}$) using the method of Do et al. [8] (see Eq. (6)).

$$\begin{aligned}\varepsilon_{tot,fre}(t_j) =& J(t_j, t_{zer})\sigma_{eff}(t_{zer}) + J(t_j - t_{zer+1}, t_{zer+1})\Delta\sigma_{eff}(t_{zer+1}) + \cdots \\ &+ J(t_j - t_j, t_j)\Delta\sigma_{eff}(t_j)\end{aligned} \tag{6}$$

Here, t_{zer} is the time zero of autogenous shrinkage and t_j is the hydration time at simulation step j.

The creep compliance was calculated as Eq. (7) [8,30,31]. In this equation, $1/E$ represents the elastic part and $ln\left(1+\frac{t_j-t_{zer}}{\tau}\right)\Big/C$ represents the creep part [8].

$$J(t_j, t_{zer}) = \frac{1}{E} + \frac{1}{C} ln\left(1 + \frac{t_j - t_{zer}}{\tau}\right) \tag{7}$$

Table 2
Calculated creep moduli of lattice elements.

Lattice elements	Calculated creep modulus (GPa)
IP-IP	190
OP-OP	135
PC-IP	311
IP-OP	233
PC-OP	158

Here, E is the Young's modulus of lattice elements, C is the creep modulus of lattice elements, and τ is the characteristic time. τ was set at 0.58 s on the basis of the experimental study of Wei et al. [31].

In the current study, the creep modulus of lattice elements was calculated from the creep modulus of connected phases using the harmonic average, wherein the creep modulus of connected phases was taken from the experimental data of Wei et al. [31]; that is, the moduli for PC, IPs and OPs were 856, 190 and 135 GPa, respectively. Table 2 gives the obtained mechanical properties of lattice elements.

(2) Total internal restraint shrinkage of lattice elements

To describe the creep behaviour of concrete, Bazant [32] proposed the concept of the effective modulus to calculate the creep of concrete from the imposed stress. The effective modulus can be calculated from the total shrinkage (i.e., the sum of the elastic part and creep part) and the imposed stress. This concept of the effective modulus has been applied in many studies for the prediction of the creep of concrete structures [33–36]. In the current study, the effective modulus of lattice elements was calculated as the effective stress and the free creep of lattice elements (Eq. (8)).

$$E_{eff}(t_j) = \sigma_{eff,i}(t_j)/\varepsilon_{tot,fre}(t_j) \tag{8}$$

The effective stress was then imposed on the lattice elements using a method similar to that described in Section 2.2, wherein the elastic moduli of lattice elements were replaced with the effective modulus. Additionally, the shear moduli of lattice elements were updated according to the ratio of the Young's modulus to the shear modulus. The total internal restraint shrinkage of lattice elements were obtained by the lattice modelling and the linear total autogenous shrinkage of cement paste ($\varepsilon_{lin,\,tot}$) (including the elastic part and creep part) was calculated as the average deformations of the nodes on surfaces divided by the size of the cement paste.

2.4. Young's modulus of the cement paste

The current study simulated the Young's modulus of cement paste following the method of Qian et al. [20,21] to determine whether the mechanical properties of the digitised cement paste are reasonable. The bottom nodes of the cement paste were first fixed. An incremental tensile displacement was then applied at the top nodes of the cement paste. The

Table 3
Chemical composition of PC determined from X-ray fluorescence.

CaO	SiO_2	Al_2O_3	Fe_2O_3	SO_3	MgO	K_2O	Na_2O	Others	LOI
63.28	20.07	4.98	3.65	2.75	1.1	0.44	0.1	0.74	2.89

Note: LOI means loss on ignition.

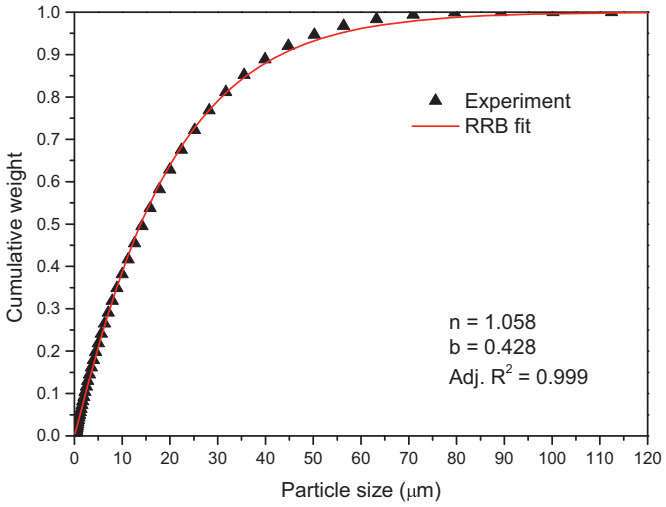

Fig. 5. Particle size distribution of PC.

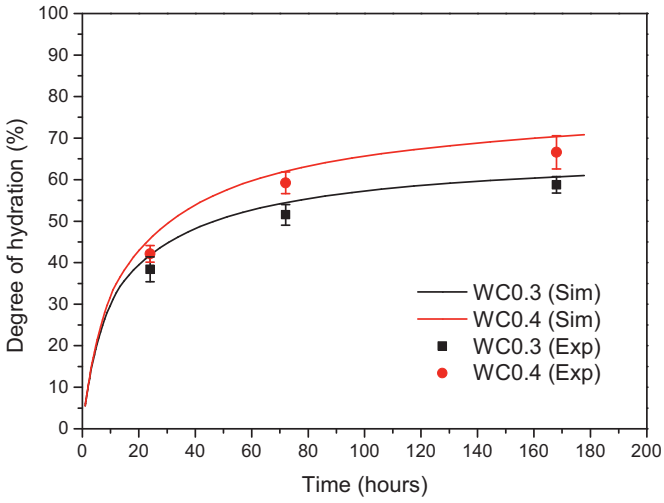

Fig. 6. Degrees of hydration of PC in WC0.3 and WC0.4.

response stresses at the top surface nodes were obtained using GLAK. The stress-strain curve of the cement paste under tensile load was obtained by increasing the tensile displacement until the system failed. The curve was then used to calculate the Young's modulus of the cement paste.

3. Experimental methods

PC pastes with W/C ratios of 0.3 and 0.4 (respectively called WC0.3 and WC0.4) were prepared to validate the modelling methods. The chemical composition of PC, which was determined from X-ray fluorescence (Axios PW4400), was used to calculate the mineral composition of PC by using the Bogue equation modified by Taylor [37]. Table 3 gives the measured chemical compositions of PC. The calculated mineral composition of PC is 72.7 % C_3S, 3.0 % C_2S, 3.3 % C_3A, 14.0 % C_4AF. Fig. 5 shows the obtained particle size distribution of PC determined through laser diffraction (Malvern Mastersizer 2000). Additionally, the particle size distribution of PC was fitted using the Rosin-Rammler-Bennet distribution: $G(x) = 1 - exp\ (-bx^n)$. $G(x)$ is the cumulative weight and x is the particle diameter. n and b are fitting parameters used as the inputs of the HYMOSTRUC3D-E model to represent the particle size distribution of PC.

The internal RH of cement paste was measured using a RH sensor based on the methods of Jensen and Hansen [38] and Huang and Ye [39]. The internal RH of each mixture was calculated as the mean value obtained in two tests. The degrees of hydration of cement were measured using the non-evaporable water method [7,40]. The degree of hydration of each mixture was calculated as the mean value for three tests. The autogenous shrinkage of cement paste was measured using a corrugated tube [7,38,39,41]. Specifically, after casting, the cement paste was poured into a corrugated tube. The corrugated tube was then sealed and immersed in an isothermal ethylene glycol bath (at 20 ± 0.5 °C). The final setting time of the cement paste, which was determined according to the European standard EN 196-3 [42], was used as the initial recording time. The autogenous shrinkage of each mixture was the mean value obtained in three tests.

The Young's modulus of cement paste was measured referring to the standard method for determining the Young's modulus of concrete under static compression (GB/T 50081-2019) [43]. The cement pastes were cast into the mould with a size of 40 × 40 × 160 mm^3. Then, the cement pastes were sealed and cured in the isothermal chamber (temperature = 20 ± 1 °C) for 24 h. After demoulding, the specimens with a size of 40 × 40 × 80 mm^3 were obtained by using a precision cutting machine to cut the cement pastes (Six specimens were obtained for each W/C). Then, the specimens were sealed by using the polyethylene film and cured in the isothermal chamber (temperature = 20 ± 1 °C) until the testing ages (1, 3, 5, and 7 days). At testing ages, three specimens were used for the axial compressive strength measurement and other three specimens were used for the Young's modulus measurement as follows: (1) The axial compressive strength of cement paste (f_{cp}), which was used as the input for the Young's modulus calculation, was obtained by applying a loading rate of 200 N/s. (2) The surfaces of the specimens for the Young's modulus measurement were grinded with the 400 mesh sand paper, and cleaned by using the ethanol. (3) The centre part of the surfaces (except for the pouring surface) were pasted on the strain gauge. (4) The specimens were loaded under a static compression at the reference load (800 N) for 90 s. Then, the compression load was increased to reach σ_a (σ_a = 1/3 of f_{cp}) with the loading rate of 200 N/s, and hold on for 90 s. After that, the compression load was reduced to the reference load with an unloading rate of 200 N/s, and held on for 60s. This process was repeated twice. During the last process, the reference load was hold on for 90s, and the load was increased to reach σ_a with the same loading rate and held on for 90 s. The Young's modulus was calculated as Eq. (9).

$$E_{pas} = \frac{\sigma_a - \sigma_0}{\varepsilon_a - \varepsilon_0} \tag{9}$$

Here E_{pas} is Young's modulus of cement paste, σ_a is the stress for the calculation of Young's modulus of cement paste, ε_a is the strain for the calculation of Young's modulus of cement paste, σ_0 and ε_0 are the stress and strain for the reference load, respectively.

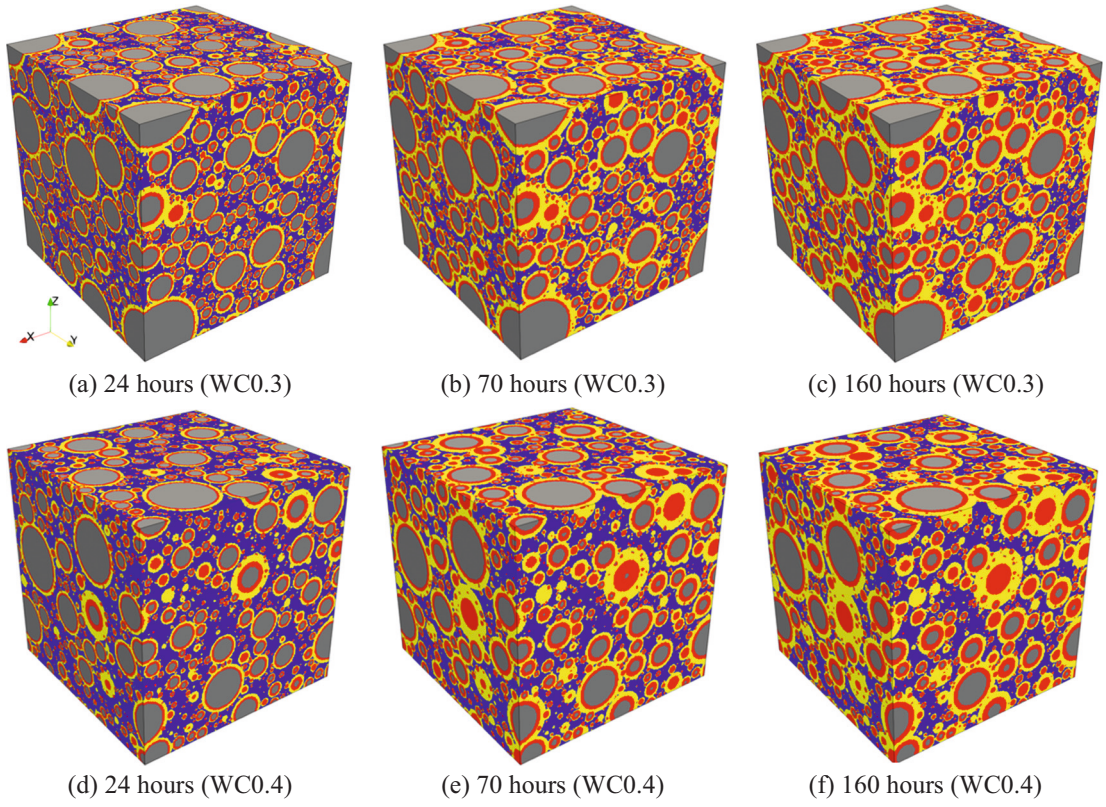

Fig. 7. Microstructures of cement pastes output by the HYMOSTRUC3D-E model: grey, red, yellow and blue respectively represent the PC, IPs, OPs and capillary pores. (For interpretation of the references to colour in this figure legend, the reader is referred to the web version of this article.)

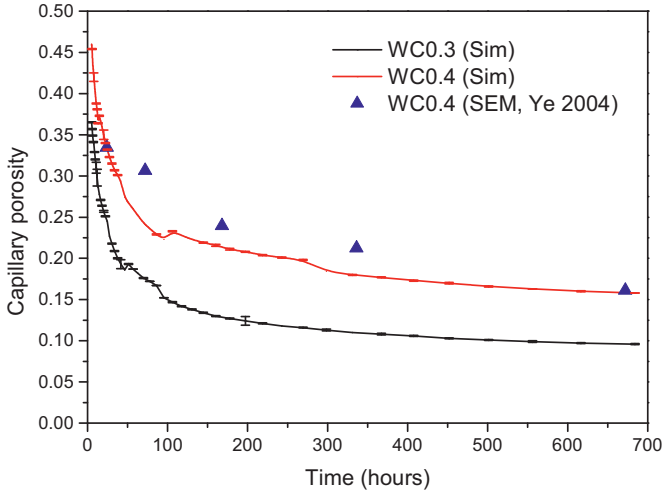

Fig. 8. Capillary porosities of WC0.3 and WC0.4.

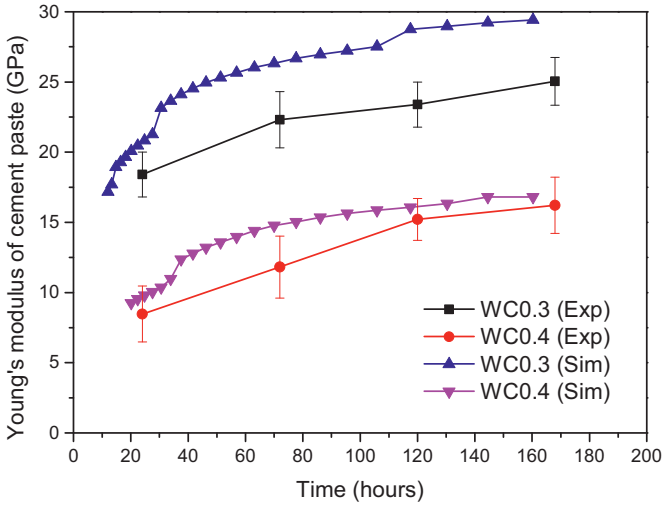

Fig. 9. Young's moduli of cement pastes obtained from simulation and experiment.

4. Results and discussion

4.1. Hydration and microstructure of the cement pastes

The simulated degree of hydration of cement and the simulated porosities and stress-strain curves of cement pastes were analysed to determine whether the microstructures of cement paste output by the HYMOSTRUC3D-E model are reasonable for modelling the shrinkage behaviour of cement paste.

As shown in Fig. 6, the degree of hydration of PC in WC0.3 increased to approximate 60 % at 168 h, which was a value smaller than that for WC0.4 (around 70 % at 168 h). These values are comparable to experiments. In HYMOSTRUC3D-E model, the reaction rate of cement is the essential for the simulation of hydration and microstructure development of cement paste. In this version of HYMOSTRUC3D-E model, to ensure that the hydration degree of PC is comparable to the experiments, the reaction rate of cement was calculated from the components of cement based on empirical equations [15,16,44], which were obtained by fitting experiment data with different components of cement. More details could be found in Appendix A.

Fig. 7 presents the microstructures of WC0.3 and WC0.4 simulated using the HYMOSTRUC3D-E model. The images show how the

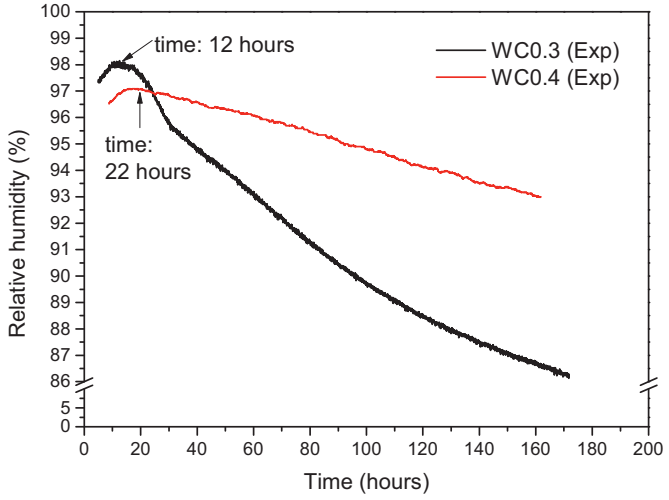

Fig. 10. Internal RH measured for WC0.3 and WC0.4.

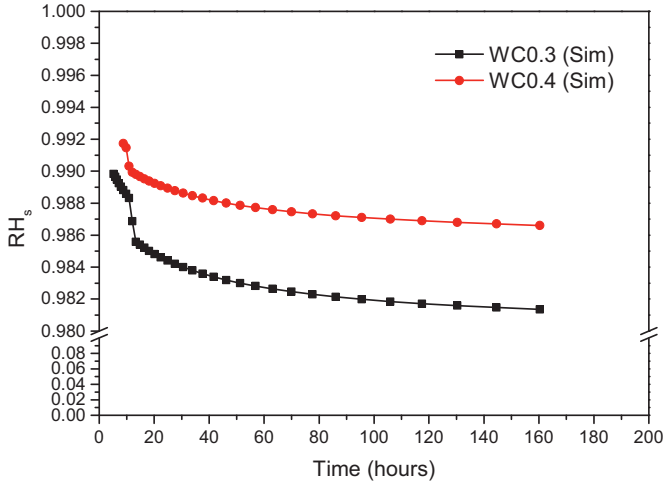

Fig. 11. RH_s calculated from the ionic concentrations of cement pastes.

microstructure of the PC paste became denser with time. The capillary porosities of WC0.3 and WC0.4 are plotted in Fig. 8. The simulated capillary porosity of WC0.4 is consistent with the scanning electron microscopy observation [45]. Notably, the capillary pores presented in this study were in microscale. In the recent studies by our group [15,16], the nanopores were also dealt with in the HYMOSTRUC3D-E model by employing the multi-scale concept and the packing of colloid particles. In these studies, the simulated porosity including the micropores and nanopores were consistent with the experimental data of MIP. However, the simulated pore size distribution was not in line with the MIP data, and was difficult to be applied in the calculation of RH following the method such as Hu et al. [46]. From the above considerations, the current study used the measured RH to calculate the driving force of autogenous shrinkage.

The simulated and measured Young's moduli of WC0.3 and WC0.4 were calculated from the data presented in Appendix B. As shown in Fig. 9, the simulated Young's moduli of WC0.3 and WC0.4 respectively reached from 20.8 to 29.4 GPa, and 12.4 to 16.2 GPa at 1 and 7 days. The values for WC0.4 are comparable to the elastic moduli of cement pastes determined by the experiments, while those for WC0.3 are slightly higher than the experiments. The literature reported similar values of the elastic moduli of cement pastes. For example, Lu et al. [7] calculated the elastic moduli of cement pastes with W/C ratios of 0.3 and 0.4 using an empirical equation proposed by Noguchi et al. [47] as approximately

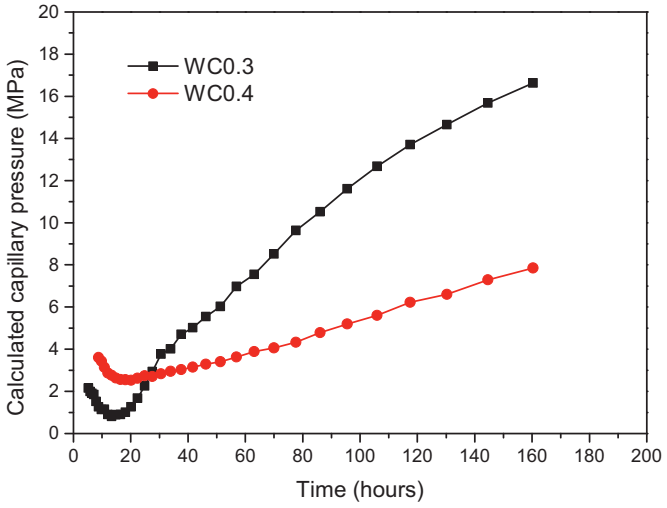

Fig. 12. Internal capillary pressures of cement pastes calculated using the Kelvin-Cohan equation.

25 and 17 GPa, respectively, at 7 days. The above comparisons show that the elastic moduli of cement pastes output by the HYMOSTRUC3D-E model are acceptable for modelling the shrinkage behaviour.

4.2. Internal RH and capillary pressure of the cement pastes

Fig. 10 presents the internal RH in WC0.3 and WC0.4 obtained using the RH sensors. For both cement pastes, the internal RH increased at an early age and then decreased with the ongoing hydration of the cement. Similar trends have been observed in other studies [3,7,39]. The initial increase in RH is probably due to that the equilibrium between the RH sensor and cement paste. Notably, the measured internal RH did not reach 100 %. This was probably due to the dissolution of salt in the pore solution [3,7]. The internal RHs of WC0.3 and WC0.4 then started to drop at approximately 12 and 20 h, respectively.

Fig. 11 shows the RH reduction factor (RH_S) calculated from the ionic concentrations of cement pastes. (The simulated ionic concentrations of cement pastes can be found in Appendix C. The method for predicting the ionic concentrations of cement pastes was validated and discussed in [16].) The RH_S decreased with the progression of hydration for both WC0.3 and WC0.4. This is because the ionic concentrations in the pore solution increased with the ongoing hydration of the cement. Additionally, because the ionic concentrations were higher in WC0.3 than in WC0.4 (see Appendix C), the RH reduction factor was greater for WC0.3 than for WC0.4. The RH_S of WC0.4 decreased to 0.986 at 160 h, which was close to the calculation of Chen et al. [48], who measured the ionic concentrations of a PC paste with a W/C of 0.4 and calculated the RH_S using the Raoult's law.

Fig. 12 shows the internal capillary pressure calculated from the internal RH and RH_S using the Kelvin-Cohan equation (Eq. (3)). After 20 h, the capillary pressure in WC0.3 was appreciably higher than that in WC0.4. At 160 h, the internal capillary pressures of WC0.3 and WC0.4 were 16.8 and 7.9 MPa, respectively. The difference in pressure was due to the measured internal RH of WC0.3 being lower than that of WC0.4. The calculated capillary pressures were consistent with values reported in other studies. Lu et al. [7], for example, measured the internal RH of PC pastes with WC ratios of 0.3 and 0.4 and calculated the internal capillary pressures. The obtained internal capillary pressures for WC ratios of 0.3 and 0.4 respectively increased to approximately 14.5 and 6 MPa at 7 days.

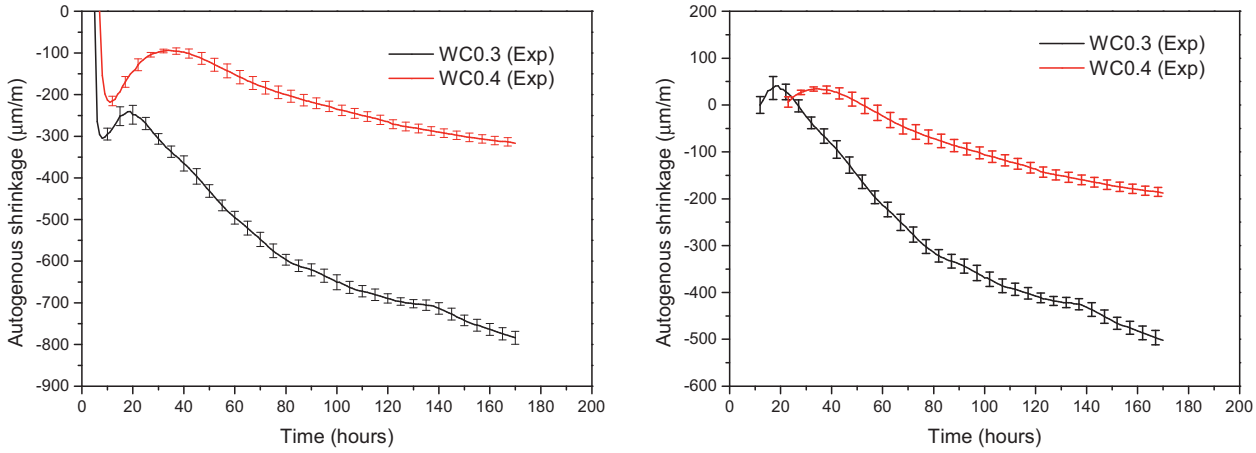

Fig. 13. Measured autogenous shrinkage of cement pastes.

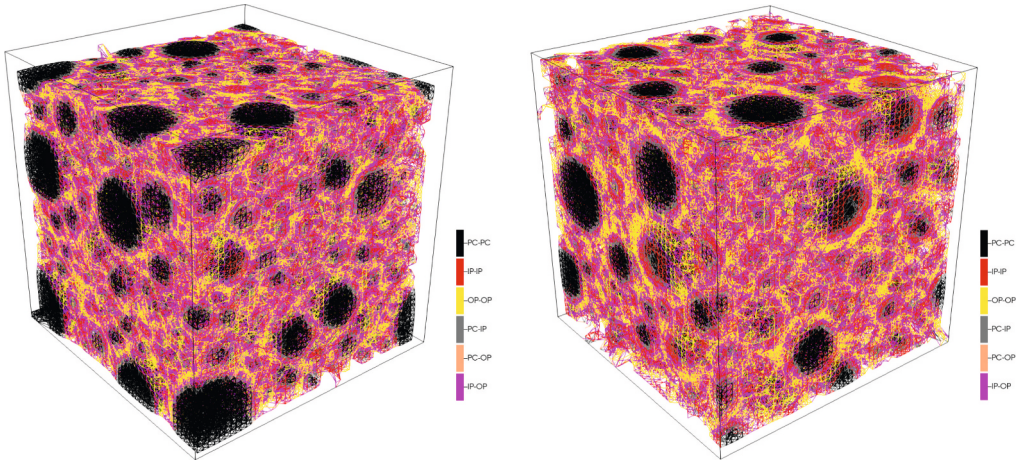

Fig. 14. Simulated 3D elastic autogenous shrinkage of cement pastes. (Deformations are magnified 400 times.)

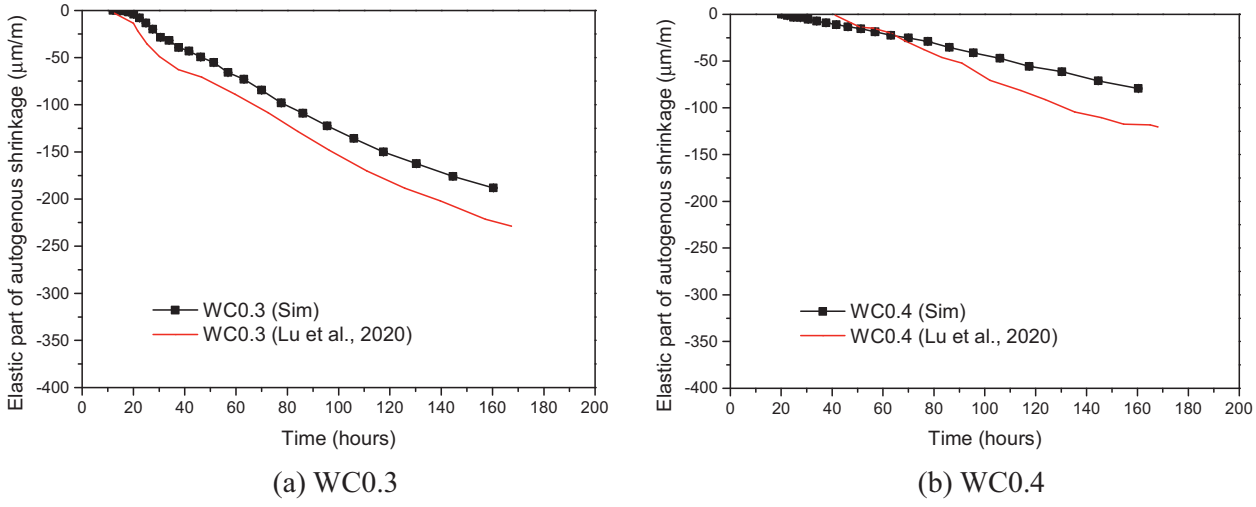

Fig. 15. Comparison of the elastic autogenous shrinkage obtained in this study and that predicted using poromechanical models (Lu et al. [7]) (with time zero being the time of the RH drop in this study and the time of maximum swelling in the study of Lu et al. [7]).

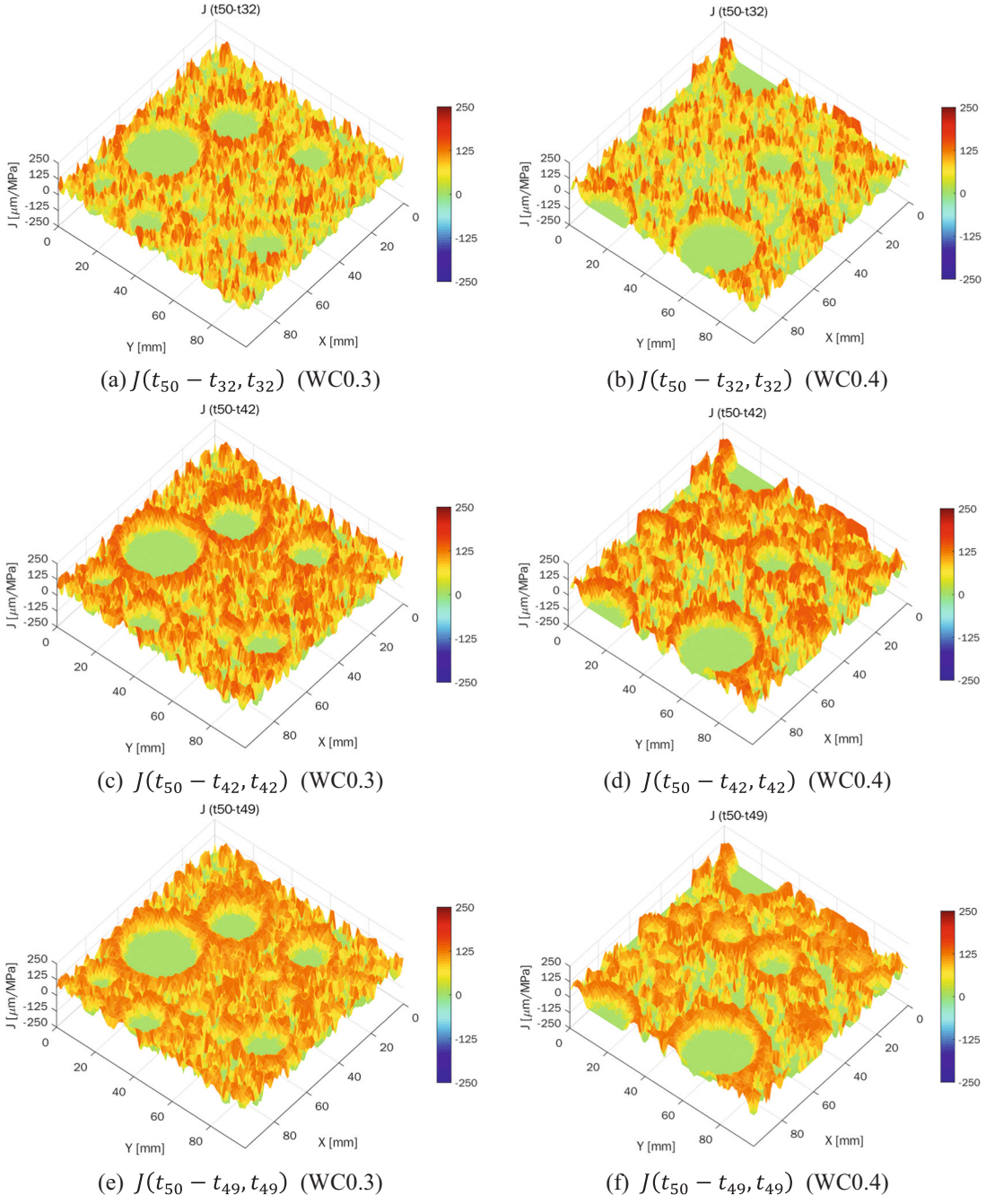

(a) $J(t_{50}-t_{32},t_{32})$ (WC0.3) (b) $J(t_{50}-t_{32},t_{32})$ (WC0.4)

(c) $J(t_{50}-t_{42},t_{42})$ (WC0.3) (d) $J(t_{50}-t_{42},t_{42})$ (WC0.4)

(e) $J(t_{50}-t_{49},t_{49})$ (WC0.3) (f) $J(t_{50}-t_{49},t_{49})$ (WC0.4)

Fig. 16. Simulated creep compliance of the lattice elements crossing the X-Y plane for $\Delta\sigma_{eff}$ at different time steps.

4.3. Measured autogenous shrinkage of the cement pastes

Fig. 13a shows the measured autogenous shrinkage of WC0.3 and WC0.4 with time zero being the final setting time (5 and 7 h for WC0.3 and WC0.4, respectively). Both cement pastes exhibited a sharp shrinkage at an early age followed by an expansion. After the expansion, the cement pastes gradually shrunk with the ongoing hydration of cement. The observed expansion is consistent with the results of Lu et al. [7] and Do et al. [8]. This expansion was probably due to the formation of crystals, such as ettringite, at an early age [1]. At 160 h, the autogenous shrinkage of WC0.3 (−764 μm/m) was larger than that of WC0.4 (−309 μm/m). Similar results were found by other researchers, such as Lu et al. [7], Do et al. [8] and Baroghel-Bouny et al. [49].

The time zero or starting point of the autogenous shrinkage of cement paste is an important research topic for the measurement of autogenous shrinkage [39,50–52]. Time zero has been set differently in different studies; for example, time zero has been the final setting time [3,6,8] and the time of maximum swelling [7]. In a recent study by Huang and Ye [39], the onset of the internal RH drop was believed to be directly linked to the start of the self-desiccation of cement paste. Thus, they recommended that the RH drop time could be the time zero of the autogenous shrinkage of cement paste. As mentioned in Section 4.2, the internal RH measured before the RH drop might not reflect the real internal RH of the cement paste. Hence, this study used the time of the RH drop as the time zero of autogenous shrinkage in validating the modelling methods. Notably, a part of the stress-induced autogenous shrinkage might be excluded by using the RH drop time as the time zero of autogenous shrinkage in the simulation. This can be avoided if the internal RH of cement paste can be obtained more accurately. Fig. 13b shows the measured autogenous shrinkage of WC0.3 and WC0.4 with

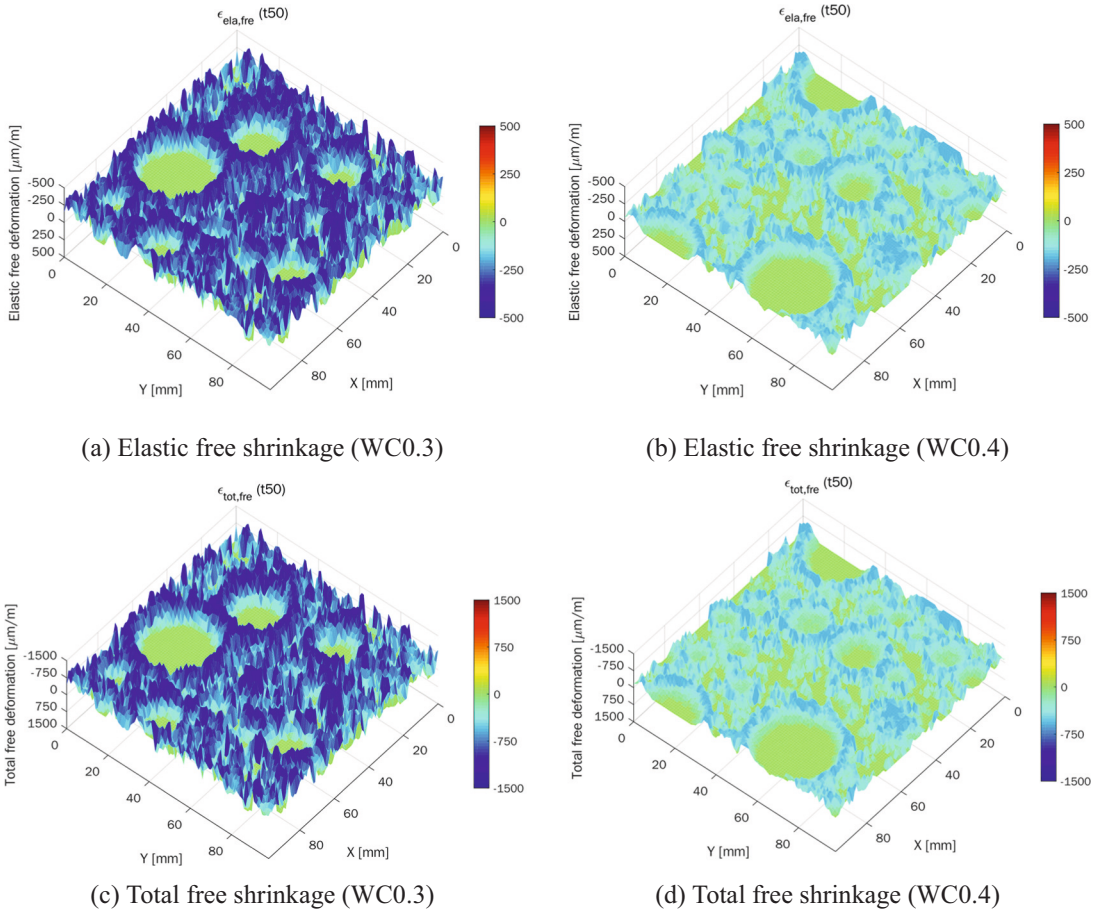

(a) Elastic free shrinkage (WC0.3)

(b) Elastic free shrinkage (WC0.4)

(c) Total free shrinkage (WC0.3)

(d) Total free shrinkage (WC0.4)

Fig. 17. Simulated elastic and total free shrinkage of lattice elements crossing the X-Y plane (at a time of 160 h).

time zero being the RH drop time (12 and 20 h for WC0.3 and WC0.4, respectively). At 160 h, the autogenous shrinkage of WC0.3 and WC0.4 reached −480 and −180 μm/m, respectively.

4.4. Simulated elastic autogenous shrinkage of the cement pastes

Fig. 14 presents the simulated 3D elastic autogenous shrinkage of WC0.3 and WC0.4 at 160 h (i.e., 50 time steps). The simulated 3D elastic autogenous shrinkage at different times can be found in Appendix D. The deformations of WC0.3 were greater than those of WC0.4. Furthermore, the shrinkage was non-uniform owing to the spatial distributions of cement particles and hydration products.

The simulated linear elastic autogenous shrinkage ($\varepsilon_{lin,\ ela}$) of cement paste is plotted in Fig. 15. It is seen that $\varepsilon_{lin,\ ela}$ of WC0.3 and WC0.4 arrived at −188 and −79 μm/m, respectively, after 160 h (i.e., 50 time steps). The obtained $\varepsilon_{lin,\ ela}$ was comparable to the values predicted using poromechanical models [7].

4.5. Simulated total autogenous shrinkage of the cement pastes

The lattice elements crossing the X-Y plane at the centre of the cement paste were considered in visualising the creep compliance, free shrinkage and total shrinkage of lattice elements.

(1) Creep compliance of lattice elements

Fig. 16 shows the creep compliance of the lattice elements crossing the X-Y plane at the centre of the cement paste. Do et al. [8] calculated the creep compliance of cement paste using a finite element method. They found that the creep compliance of cement paste was in the range of 0–500 μm/MPa, depending on the initial loading time and the final loading time. In the current study, the initial loading time was t_{32} (24 h) and the finial loading time was t_{50} (160 h) for the effective stress $\Delta\sigma_{eff}(t_{32})$ from t_{31} to t_{32}. Fig. 16a shows that the distribution of creep compliance was relatively sparse. For the effective stress $\Delta\sigma_{eff}(t_{49})$ from t_{48} to t_{49}, the initial loading time was t_{49} (145 h) and the finial loading time was t_{50} (160 h). The obtained distribution of creep compliance is presented in Fig. 16e. It is seen that the distribution of creep compliance was dense. This is because the distribution of hydration products affects the distribution of creep compliance (i.e., there are more hydration products in Fig. 16e). Furthermore, the distributions of creep compliance in WC0.4 were sparse owing to the less formation of hydration products (see Fig. 16b, d and f). The obtained creep compliance was used to calculate the free total autogenous shrinkage of lattice elements (see Eq. (6)).

(2) Elastic and total free shrinkage of lattice elements

Fig. 17 shows the simulated elastic and total free shrinkage of the lattice elements crossing the X-Y plane at the centre of the cement paste (at a time of 160 h). The total free shrinkage including the elastic part and creep part was almost three times the elastic free shrinkage (see the colour bar in Fig. 17). Both the elastic free shrinkage and total free shrinkage were non-uniform owing to the random distribution of cement particles. WC0.3 had much larger elastic free shrinkage and total free shrinkage than WC0.4. The obtained total free shrinkage of lattice elements was used to calculate the effective modulus of lattice elements (see Eq. (8)).

(3) Elastic and effective moduli of lattice elements

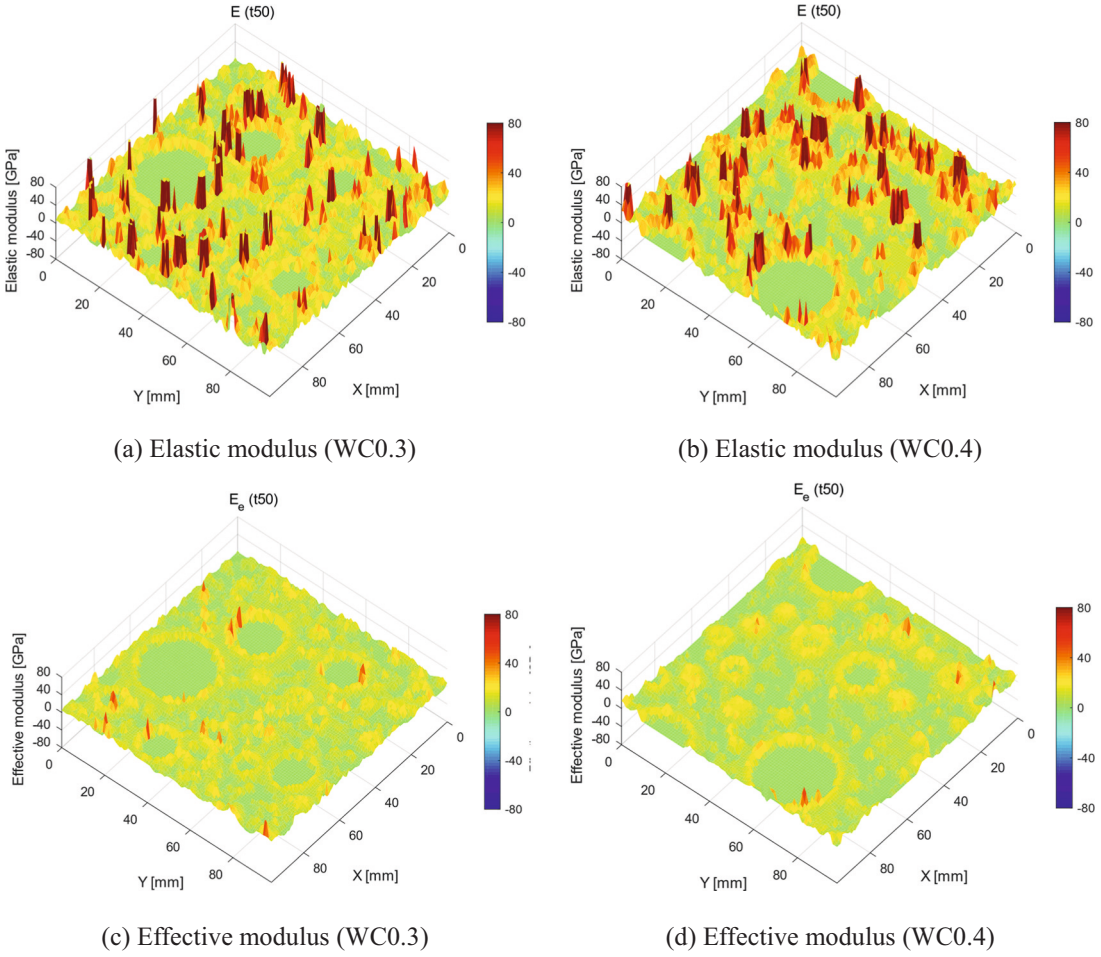

(a) Elastic modulus (WC0.3) (b) Elastic modulus (WC0.4)

(c) Effective modulus (WC0.3) (d) Effective modulus (WC0.4)

Fig. 18. Elastic and effective moduli of lattice elements crossing the X-Y plane (at a time of 160 h). Note that, to focus on the properties of the lattice elements of the hydration products, the elastic and effective moduli of the PC-PC lattice elements are not shown.

Fig. 18a and b shows the Young's modulus of the lattice elements crossing the X-Y plane at the centre of the cement paste whereas Fig. 18c and d shows the calculated effective modulus of the lattice elements. It is seen that the elastic and effective moduli of lattice elements were non-uniform, and the effective modulus was much smaller than the Young's modulus because the effect of creep was considered in calculating the effective modulus (see Eqs. (6) and (8)). As described in Section 2.3, the obtained effective modulus was applied in the lattice fracture to simulate the total restrained shrinkage of the cement paste.

(4) Elastic and total internal restraint shrinkage of lattice elements

Fig. 19 shows the simulated elastic and total internal restraint shrinkage of the lattice elements crossing the X-Y plane at the centre of the cement paste (at a time of 160 h). The elastic free shrinkage and total free shrinkage were redistributed owing to the restraint of the unreacted PC phase. It is seen that the shrinkage of lattice elements was non-uniform. Some lattice elements had tensile strains because of the restraining effect of unreacted PC on the free shrinkage of lattice elements.

Fig. 20 shows the simulated 3D total autogenous shrinkage of WC0.3 and WC 0.4 at 160 h (i.e., 50 time steps). The deformations of WC0.3 were greater than those of WC0.4. Additionally, the deformations are non-uniform owing to the random distribution of cement particles. The simulated 3D total autogenous shrinkage at different times can be found in Appendix E.

Fig. 21 shows that the simulated total autogenous shrinkage of WC0.3 and WC0.4 reached −501 and −236 μm/m, respectively, at 160 h. These values are in good agreement with the experimental data (−480 and −180 μm/m for WC0.3 and WC0.4, respectively, at 160 h). However, the evolution of the simulated autogenous shrinkage was slightly different from that of the measured autogenous shrinkage. First, the expansion observed in the experiment did not exist in the simulation. This is because the expansion mechanism, probably the formation pressure of crystals such as ettringite, was not considered in the simulation. After the expansion, the evolution of the autogenous shrinkage measured using the corrugated tube method was more rapid than that of the autogenous shrinkage obtained in the simulation. One possible reason is that the Poisson ratios of hydration products change with the ongoing hydration of cement [30] whereas the Poisson ratios of hydration products were set constant in the current study. According to Eqs. (1) and (2), the Poisson ratios of hydration products might affect the effective stress imposed on the hydration products. Consequently, both the elastic part and creep part of autogenous shrinkage could change.

4.6. *Practical importance of the current study and further work*

The current study established a modelling framework for simulating the 3D autogenous shrinkage of cement paste. The elastic part and creep part of autogenous shrinkage were directly quantified and visualised. The HYMOSTRUC3D-E model was used to obtain the 3D microstructure and the ionic concentrations of cement paste. Other cement hydration models, such as CEMHYD3D [53] and μic [54], have functions similar to the HYMOSTRUC3D-E model. By applying these hydration models in the

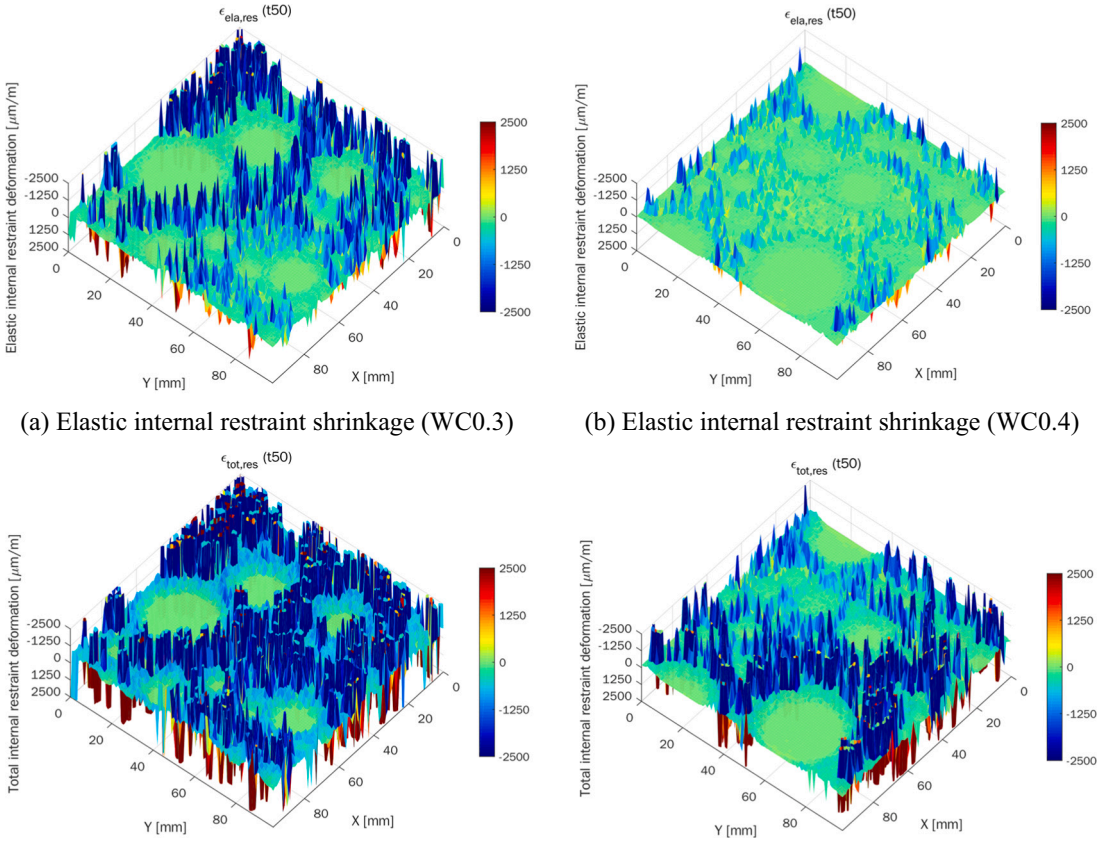

(a) Elastic internal restraint shrinkage (WC0.3) (b) Elastic internal restraint shrinkage (WC0.4)

(c) Total internal restraint shrinkage (WC0.3) (b) Total internal restraint shrinkage (WC0.4)

Fig. 19. Simulated elastic and total internal restraint shrinkage of lattice elements crossing the X-Y plane (at a time of 160 h).

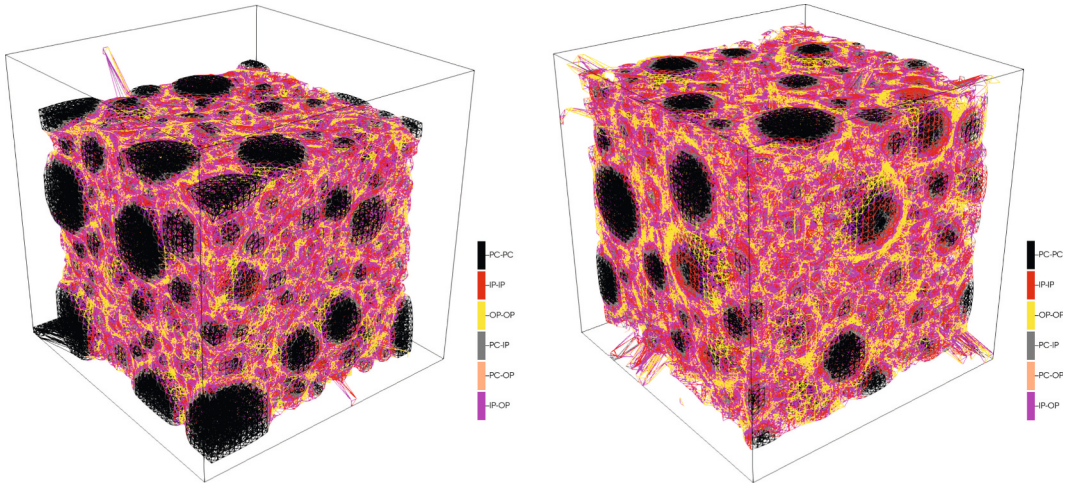

(a) WC0.3 (b) WC0.4

Fig. 20. Simulated 3D total deformations (elastic part + creep part) of cement pastes. (Deformations are magnified 400 times.)

current modelling framework, the effects of the W/C ratio and components of cements (e.g., the contents of blast furnace slag and fly ash) on the 3D autogenous shrinkage of cement paste could be analysed. In addition, the volume fraction and the stiffness of the cement particles play important roles on the restraining effect of unreacted phase on the local shrinkage of hydration products. These aspects can be quantified in the current modelling framework because the HYMOSTRUC3D-E model can obtain the microstructure of cement pastes with different volume fractions of cement, and the lattice model can deal with the lattice elements with different stiffness. The simulated autogenous shrinkage of cement paste can be taken as input in evaluating the autogenous shrinkage of concrete in the multi-scale modelling framework.

Notably, the RH is an important input to calculate the driving force of autogenous shrinkage in this model. In the study like Hu et al. [46], the

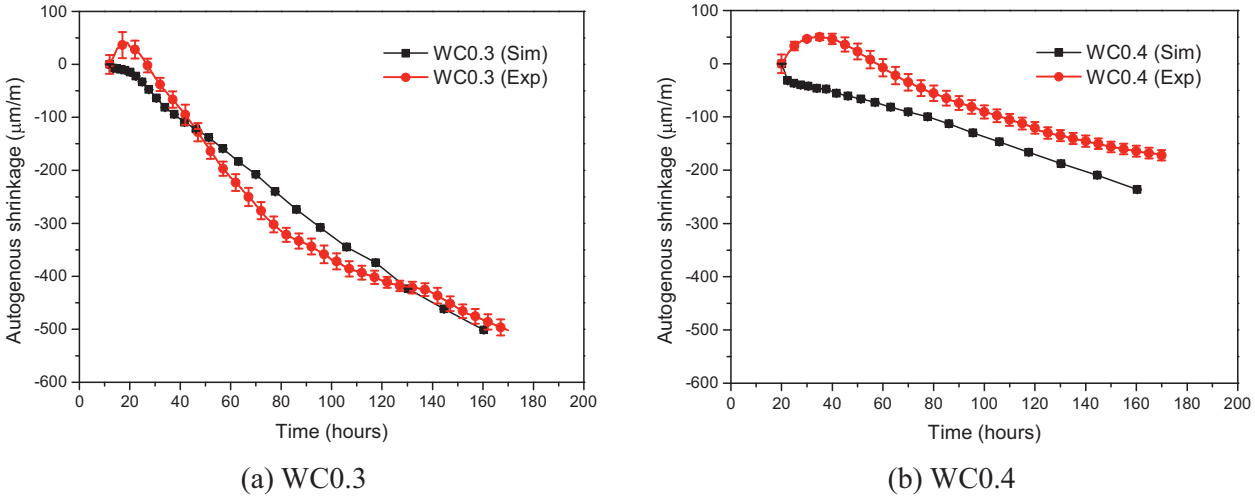

Fig. 21. Comparison of total autogenous shrinkage between simulation and experiment (with time zero being the time of the RH drop).

ionic concentrations can be used to calculate the ionic strength, which can be applied to accurately quantify influence of ions on the RH, rather than using the Raoult's law. This is also an important aspect should be considered in further model. As previously mentioned, the evolution of the simulated total autogenous shrinkage was slightly different from that in the experiments. One possible reason is that the formation pressure of crystals or the dynamic change in the Poisson ratios of hydration products was not involved in the current modelling frame. Moreover, the method for obtaining local Young's modulus and creep modulus of cement paste should also be concerned because they are also important for affecting the prediction of autogenous shrinkage. These points should be explored in further work. Furthermore, the cement particles are irregularly shaped, which might also affect the restraining effect of the unreacted phase on the local shrinkage of hydration products. However, this effect was not quantified in the current modelling framework because the cement particles were assumed to be spherical in the HYMOSTRU3D-E model [15,16]. This effect could be considered using a cement hydration model with irregularly shaped cement particles such as CEMHYD3D or incorporating a model of irregularly shaped particles (e.g., the Anm materials model [19]) in the HYMOSTRUC3D-E model.

5. Conclusions

A structure-based modelling framework was established to deal with both the elastic part and creep part in the 3D autogenous shrinkage of cement paste. The hydration, microstructure and ionic concentrations of cement paste were obtained using the HYMOSTRUC3D-E model. The stress, which was calculated from the measured internal RH of cement paste based on the concept of effective stress, was imposed on the hydration products using the lattice fracture model. The creep compliance involving the elastic part and creep part was used to calculate the total free shrinkage of hydration products. The obtained total free shrinkage of hydration products was used to calculate the effective moduli of hydration products, which were used as inputs of the lattice fracture model to simulate the 3D autogenous shrinkage of cement paste.

To validate the modelling framework, PC pastes with a W/C ratio of 0.3 (WC0.3) and 0.4 (WC0.4) were prepared and their autogenous shrinkage was determined using a corrugated tube. At 160 h, the linear elastic autogenous shrinkage of WC0.3 and WC0.4 reached −188 and −79 μm/m, respectively (with time zero being the RH drop time). These values are comparable to the values predicted using poromechanical models. The simulated linear total autogenous shrinkage of WC0.3 and WC0.4 reached −501 and −236 μm/m, respectively (with time zero being the RH drop time), which are close to values measured using the corrugated tube. The above comparisons validate the proposed structure-based modelling frame for predicting the 3D autogenous shrinkage of cement paste.

The main limitation of this modelling framework is that the internal RH of cement paste, which was the key input for calculating the driving force of shrinkage, was obtained from the experiments rather than from simulation. This is because the pore size distribution simulated by the current version of HYMOSTRUC3D-E model was inconsistent with the reality. Consequently, it was difficult to predict the internal RH of cement paste in the current modelling frame work. This limitation can be solved if a more sophisticated cement hydration and microstructure development model is developed in further work.

CRediT authorship contribution statement

Peng Gao: Visualization, Writing - original draft, Writing - review & editing. **Guang Ye**: Software. **Haoliang Huang**: Writing - review & editing. **Zhiwei Qian**: Software. **Erik Schlangen**: Software. **Jiangxiong Wei**: Conceptualization, Supervision, Writing - review & editing. **Qijun Yu**: Supervision.

Declaration of competing interest

The authors declare that they have no known competing financial interests or personal relationships that could have appeared to influence the work reported in this paper.

Acknowledgements

This work was supported by the National Key Research and Development Program (2020YFC1909903), the National Natural Science Foundation of China (Grant No. 51772103, 51872097, and 52002129).

Appendix A. Hydration parameters of the HYMOSTRUC3D-E model

In the HYMOSTRUC3D-E model, the hydration rates of the components of PC particles (C_3S, C_2S, C_3A and C_4AF) are simulated using Eq. (A.1).

$$\frac{\Delta\delta_{in,x_i,j+1,M_k}}{\Delta t_{j+1}} = K_{0,M_k} \times \Omega_1(.) \times \Omega_2(.) \times \Omega_3(.) \times F_1(.) \times \left[F_2(.) \times \left(\frac{\delta_{tr,M_k}}{\delta_{x_i,j,M_k}} \right)^{\beta_1} \right]^{\lambda_{M_k}} \tag{A.1}$$

Here, $\Delta\delta_{in,\,x_i,\,j+1,\,M_k}$ is an incremental increase in the penetration depth of the reacted part of component M_k ($M_{k=1} = C_3S$; $M_{k=2} = C_2S$; $M_{k=3} = C_3A$; $M_{k=4} = C_4AF$) during a time increment $\Delta t_{j+1} = t_{j+1} - t_j$. $K_{0,\,M_k}$ and δ_{tr} are two important model parameters. $K_{0,\,M_k}$ is the initial penetration rate of the reaction front of component M_k (μm/h). $\delta_{tr,\,M_k}$ is the transition thickness of the shell of hydration products when the hydration mechanism of M_k changes from a *phase boundary reaction* ($\lambda_{M_k} = 0$) to a *diffusion-controlled reaction* ($\lambda_{M_k} = 0$). δ_{tr} is the transition thickness of the shell of hydration products when the hydration mechanism of a PC particle changes from a *phase boundary reaction* to a *diffusion-controlled reaction*. The values of K_0 and δ_{tr} for C_3S, C_2S, C_3A and C_4AF are calculated from the components of cement using the empirical equations suggested by Tuan [44]. The definitions of other parameters in Eq. A.1 can be found in the literature [15,16]. Table A.1 gives the calculated modelling parameters.

Table A.1
Modelling parameters of HYMOSTRUC3D-E.

Phase	K_0 [μm/h]	δ_{tr} [μm]
C_3S	0.072	2.73
C_2S	0.005	3.07
C_3A	0.122	3.51
C_4AF	0.020	1.19

Fig. A.1 shows the hydration time versus the time step for the HYMOSTRUC3D-E model.

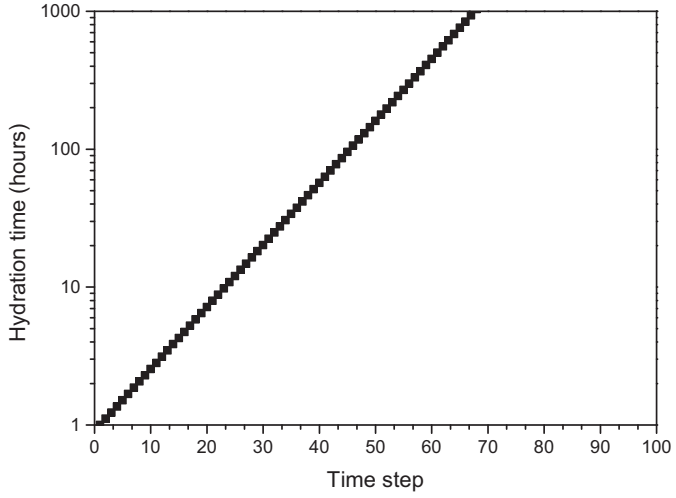

Fig. A.1. Hydration time versus time step for the HYMOSTRUC3D-E model.

Appendix B. Loading curves for determining the Young's moduli of cement pastes

Fig. B.1 and B.2 show the curves for calculating the simulated and measured Young's moduli of cement pastes.

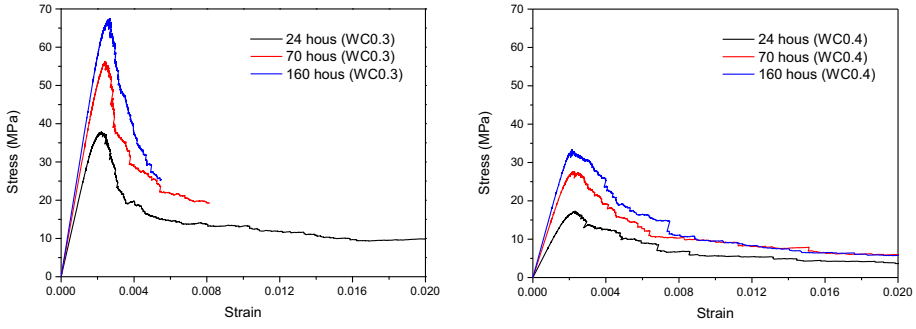

(a) WC0.3 (b) WC0.4

Fig. B.1. Simulated stress-strain curves of cement pastes under a tensile load.

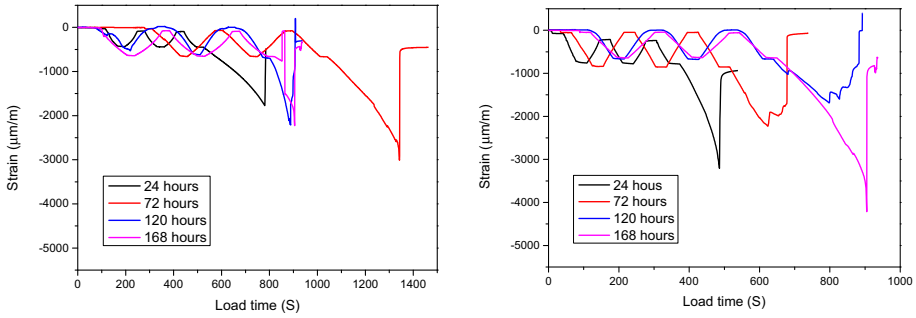

(a) WC0.3 (b) WC0.4

Fig. B.2. Loading curves for determining the Young's moduli of cement pastes.

Appendix C. Ionic concentrations of the cement paste simulated using the HYMOSTRUC3D-E model

Tables C.1 and C.2 respectively show the simulated ionic concentrations of WC0.3 and WC0.4.

Table C.1
Ionic concentrations of WC0.3 simulated using the HYMOSTRUC3D-E model.

Step	Time (hours)	Ions' concentrations (mol/L)					pH
		Na^+	K^+	Ca^{2+}	SO_4^{2-}	OH^-	
1	1.00	0.04	0.23	0.0044	0.087	0.11	13.04
12	3.13	0.05	0.26	0.0041	0.099	0.12	13.07
17	5.25	0.06	0.28	0.0038	0.109	0.12	13.09
24	10.84	0.07	0.32	0.0033	0.130	0.13	13.13
32	24.83	0.08	0.36	0.0003	0.000	0.44	13.64
42	69.98	0.09	0.40	0.0002	0.000	0.50	13.70
50	160.32	0.10	0.43	0.0002	0.000	0.53	13.72

Table C.2
Ionic concentrations of WC0.4 simulated using the HYMOSTRUC3D-E model.

Step	Time (hours)	Ionic concentrations (mol/L)					pH
		Na^+	K^+	Ca^{2+}	SO_4^{2-}	OH^-	
1	1.00	0.03	0.17	0.0056	0.060	0.09	12.98
12	3.13	0.04	0.19	0.0052	0.068	0.10	13.00
17	5.25	0.04	0.20	0.0049	0.074	0.10	13.02
24	10.84	0.05	0.23	0.0008	0.014	0.25	13.40
32	24.83	0.06	0.25	0.0005	0.000	0.31	13.49
42	69.98	0.07	0.28	0.0004	0.000	0.35	13.55
50	160.32	0.08	0.30	0.0004	0.000	0.38	13.58

Appendix D. Three-dimensional elastic autogenous shrinkage of cement pastes at different times

Fig. D.1 shows the simulated 3D elastic autogenous shrinkage of WC0.3 and WC0.4 at different times.

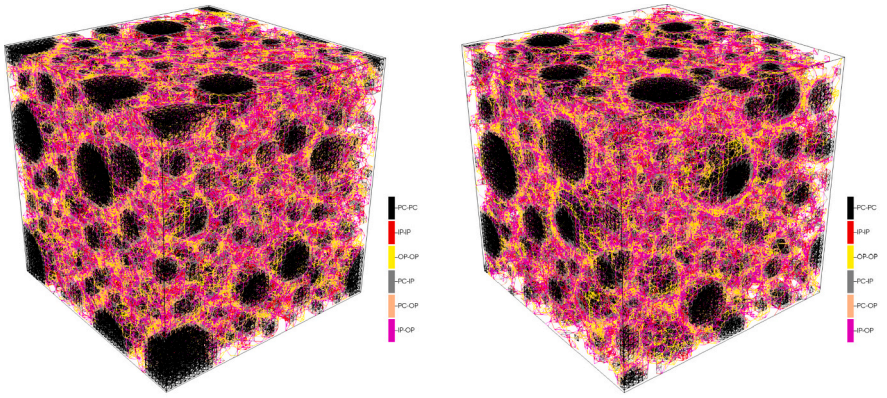

(a) 24 hours (WC0.3) (b) 24 hours (WC0.4)

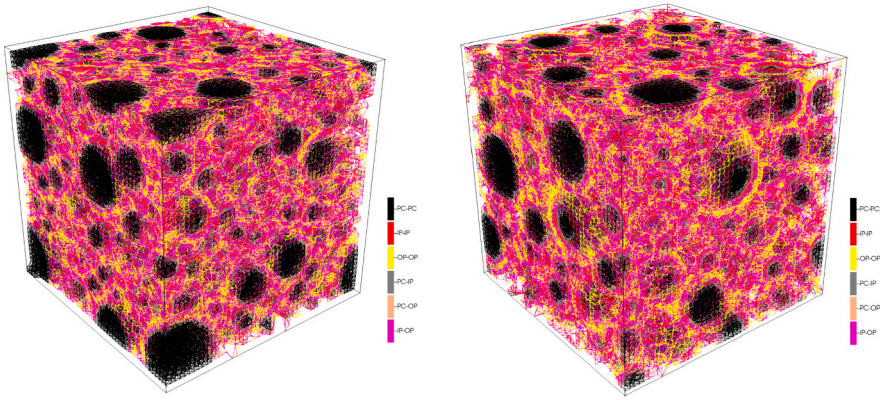

(c) 70 hours (WC0.3) (d) 70 hours (WC0.4)

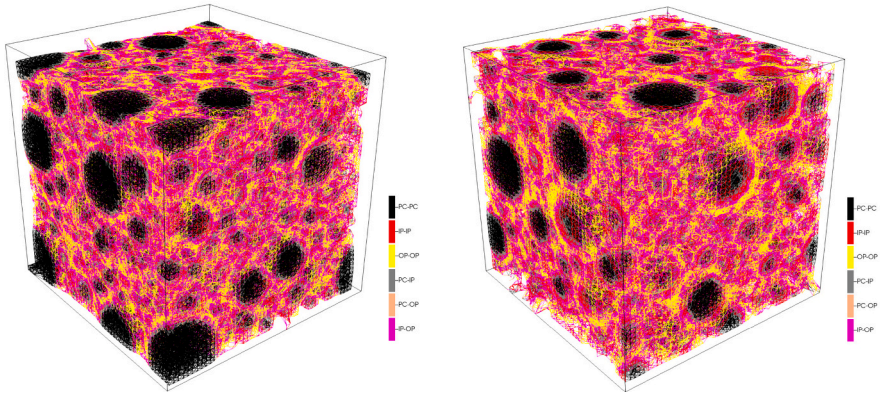

(e) 160 hours (WC0.3) (f) 160 hours (WC0.4)

Fig. D.1. Three-dimensional elastic deformations of WC0.3 and WC0.4 at different times. (Deformations are magnified 400 times.)

Appendix E. Three-dimensional total autogenous shrinkage of cement pastes at different times

Fig. E.1 shows the simulated 3D total autogenous shrinkage of WC0.3 and WC0.4 at different times.

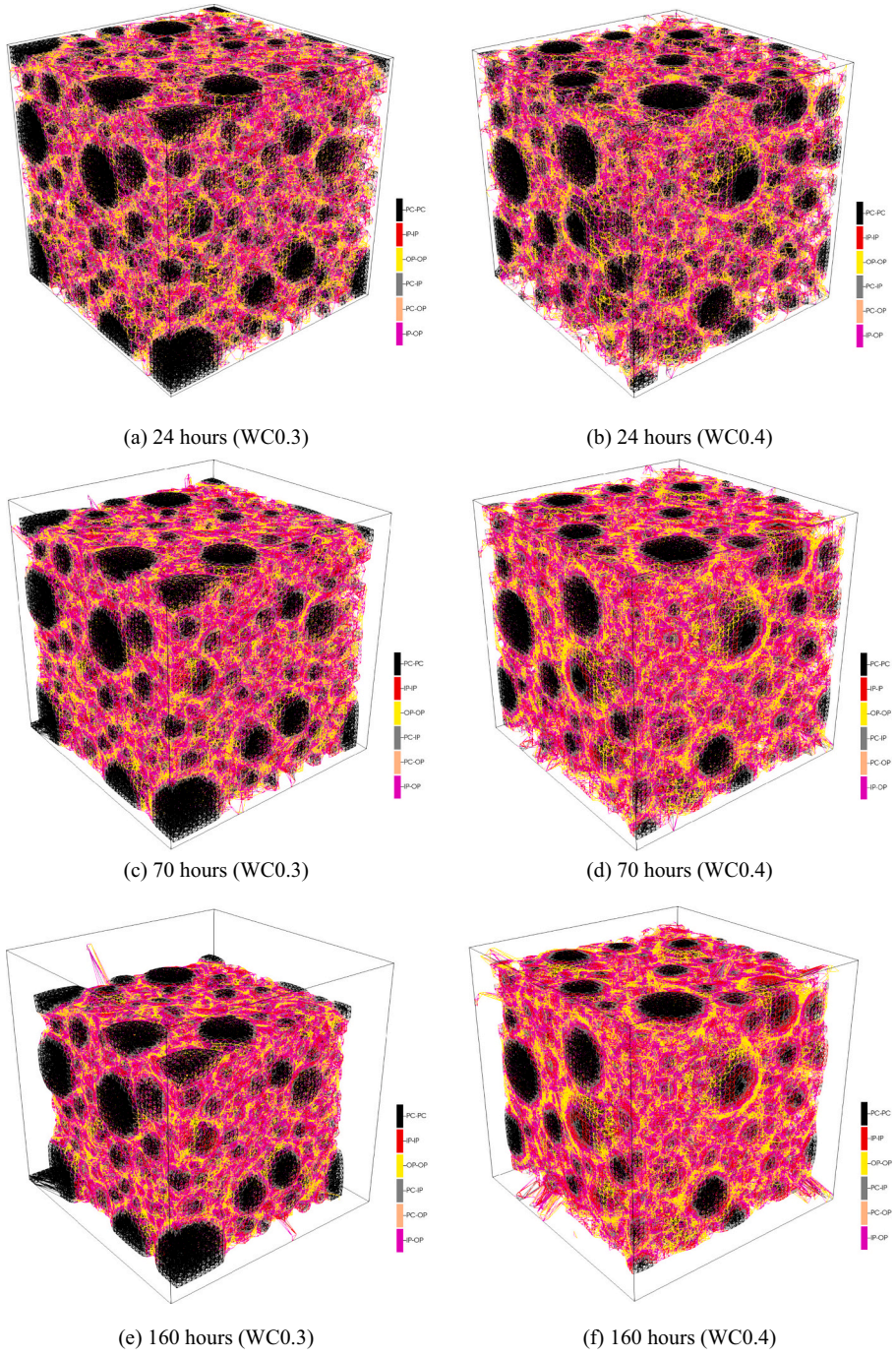

(a) 24 hours (WC0.3) (b) 24 hours (WC0.4)

(c) 70 hours (WC0.3) (d) 70 hours (WC0.4)

(e) 160 hours (WC0.3) (f) 160 hours (WC0.4)

Fig. E.1. Three-dimensional elastic and creep deformations of WC0.3 and WC0.4 at different times. (Deformations are magnified 400 times.)

References

[1] D.P. Bentz, O.M. Jensen, Mitigation strategies for autogenous shrinkage cracking, Cem. Concr. Compos. 26 (2004) 677–685.
[2] E. Holt, Contribution of mixture design to chemical and autogenous shrinkage of concrete at early ages, Cem. Concr. Res. 35 (2005) 464–472.
[3] P. Lura, O.M. Jensen, K.V. Breugel, Autogenous shrinkage in high-performance cement paste: an evaluation, Cem. Concr. Res. 33 (2003) 223–232.
[4] C. Hua, A. Ehrlacher, P. Acker, Analyses and models of the autogenous shrinkage of hardening cement paste II. Modelling at scale of hydrating grains, Cem. Concr. Res. 27 (1997) 245–258.
[5] P. Gao, G. Ye, J. Wei, Q. Yu, Numerical simulation of the autogenous shrinkage of hardening Portland cement paste, ECCOMAS Congress 2016, in: VIT European Congress of Computational Methods in Applied Sciences and Engineering, Crete Island, Greece, 2016.
[6] Z. Hu, M. Wyrzykowski, K. Scrivener, P. Lura, Prediction of autogenous shrinkage of cement pastes as poro-visco-elastic deformation, Cem. Concr. Res. 126 (2019), 105917.
[7] T. Lu, Z. Li, K.V. Breugel, Modelling of autogenous shrinkage of hardening cement paste, Constr. Build. Mater. 264 (2020), 120708.
[8] H.Q. Do, S. Bishnoi, K.L. Scrivener, Microstructural modelling of autogenous shrinkage in Portland cement paste at early age, Eng. Comput. 37 (2020) 3171–3186.
[9] C. Pichler, R. Lackner, H.A. Mang, A multiscale micromechanics model for the autogenous-shrinkage deformation of early-age cement-based materials, Eng. Fract. Mech. 74 (2007) 34–58.

[10] H. Zhao, J. Liu, X. Yin, Y. Wang, D. Huang, A multiscale prediction model and simulation for autogenous shrinkage deformation of early-age cementitious materials, Constr. Build. Mater. 215 (2019) 482–493.
[11] D. Gawin, F. Pesavento, B.A. Schrefler, Hygro-thermo-chemo-mechanical modelling of concrete at early ages and beyond. Part II: shrinkage and creep of concrete, Int. J. Numer. Meth. Engng. 67 (2006) 332–363.
[12] M. Wyrzykowski, P. Lura, F. Pesavento, D. Gawin, Modeling of internal curing in maturing mortar, Cem. Concr. Res. 41 (2011) 1349–1356.
[13] D.P. Bentz, E.J. Garboczi, D.A. Quenard, Modelling drying shrinkage in reconstructed porous materials: application to porous vycor glass, Model. Simul. Mater. Sci. Eng. 6 (1999) 211–236.
[14] L. Liu, X.C. Wang, H.S. Chen, C.J. Wan, Microstructure-based modelling of drying shrinkage and microcracking of cement paste at high relative humidity, Constr. Build. Mater. 126 (2016) 410–425.
[15] P. Gao, Simulation of Hydration and Microstructure Development of Blended Cements, PhD Thesis, Delft University of Technology, Delft, The Netherlands, 2018.
[16] P. Gao, G. Ye, J. Wei, Q. Yu, Extension of Hymostruc3D model for the simulation of hydration and microstructure development of blended cements, HERON 64 (2019) 125–148.
[17] H.F.W. Taylor, A method for predicting alkali ion concentrations in cement pore solutions, Adv. Cem. Res. 1 (1987) 5–17.
[18] Z. Qian, E. Schlangen, G. Ye, K.V. Breugel, Prediction of mechanical properties of cement paste at microscale, Mater. Constr. 60 (2010) 7–18.
[19] Z. Qian, Multiscale Modelling of Fracture Processes in Cementitious Materials, PhD Thesis, Delft University of Technology, Delft, The Netherlands, 2012.
[20] Z. Qian, E. Schlangen, G. Ye, K.V. Breugel, Modeling framework for fracture in multiscale cement-based material structures, Materials 10 (2017) 587.
[21] H. Zhang, B. Šavija, S.C. Figueiredo, M. Lukovic, E. Schlangen, Microscale testing and modelling of cement paste as basis for multi-scale modelling, Materials 9 (2016) 907.
[22] H. Zhang, B. Šavija, S.C. Figueiredo, E. Schlangen, Experimentally validated multi-scale modelling scheme of deformation and fracture of cement paste, Cem. Concr. Res. 102 (2017) 175–186.
[23] H. Zhang, Y. Xu, Y. Gan, Z. Chang, E. Schlangen, B. Šavija, Combined experimental and numerical study of uniaxial compression failure of hardened cement paste at micrometre length scale, Cem. Concr. Res. 126 (2019), 105925.
[24] M. Luković, B. Šavija, E. Schlangen, G. Ye, K.V. Breugel, A 3D lattice modelling study of drying shrinkage damage in concrete repair systems, Materials 9 (2016) 575.
[25] B. Šavija, J. Pacheco, E. Schlangen, Lattice modeling of chloride diffusion in sound and cracked concrete, Cem. Concr. Compos. 42 (2013) 30–40.
[26] A.W. Skempton, Effective Stress in Soils, Concrete and Rocks, Pore Pressure and Suction in Soils, in: Butherworths, London, 1961, pp. 4–16.
[27] H.M. Jennings, Refinements to colloid model of C-S-H in cement: CM-II, Cem. Concr. Res. 38 (2008) 275–289.
[28] A. Aili, M. Vandamme, J.M. Torrenti, B. Masson, J. Sanahuja, Time evolutions of non-aging viscoelastic Poisson's ratio of concrete and implications for creep of C-S-H, Cem. Concr. Res. 90 (2016) 144–161.
[29] P. Lura, B. Lothenbach, Influence of pore solution chemistry on shrinkage of cement paste, in: The 50-year Teaching and Research Anniversary of Prof. Sun Wei on Advances in Civil Engineering Materials, 15 October 2008, pp. 191–200. Nanjing, China.
[30] M. Vandamme, C.A. Tweedie, G. Constantinides, F.J. Ulm, K. Vliet, Quantifying plasticity-independent creep compliance and relaxation of viscoelastoplastic materials under contact loading, J. Mater. Res. 27 (2012) 302–312.
[31] Y. Wei, S. Liang, X. Gao, Indentation creep of cementitious materials: experimental investigation from nano to micro length scales, Constr. Build. Mater. 143 (2017) 222–233.
[32] Z.P. Bazant, Prediction of concrete creep effects using age-adjusted effective modulus method, J. Am. Concr. Inst. 69 (1972) 212–217.
[33] A.E. Naaman, Time-dependent deflection of prestressed beams by the pressure-line method, PCI J. 28 (1983) 98–119.
[34] Q. Yu, Z.P. Bazant, R. Wan-Wendner, Improved algorithm for efficient and realistic creep analysis of large creep-sensitive concrete structures, ACI Struct. J. 109 (2012) 665–676.
[35] M.A. Bradford, Y.L. Pi, W. Qu, Time-dependent in-plane behaviour and buckling of concrete-filled steel tubular arches, Eng. Struct. 33 (2011) 1781–1795.
[36] Z.Q. Cheng, R. Zhao, Y. Yuan, F. Li, T. Xu, Ageing coefficient for early age tensile creep of blended slag and low calcium fly ash geopolymer concrete, Constr. Build. Mater. 262 (2020), 119855.
[37] H.F.W. Taylor, Modification of the Bogue calculation, Adv. Cem. Res. 2 (1989) 73–77.
[38] O.M. Jensen, P.F. Hansen, Autogenous deformation and RH-change in perspective, Cem. Concr. Res. 31 (2001) 1859–1865.
[39] H. Huang, G. Ye, Examining the "time-zero" of autogenous shrinkage in high/ultra-high performance cement paste, Cem. Concr. Res. 97 (2017) 107–114.
[40] L. Molina, On predicting the influence of curing conditions on the degree of hydration, Swedish Cement and Concrete Research Institute, 1992.
[41] ASTM C 1698-09 (Reapproved 2014), Standard Test Method for Autogenous Strain of Cement Paste and Mortar, American Society for Testing and Materials, New York, 2014.
[42] EN 196-3, Methods of Testing Cement-Part 3: Determination of Setting Time and Soundness, British Standards Institution, London, 2005.
[43] GB/T 50081-2019, Standard for test method of physical and mechanical properties on concrete, in: China National Standards, 2019.
[44] N.V. Tuan, Rice husk ash as a mineral admixture for ultra high performance concrete, Delft, Delft University of Technology, The Netherlands, 2011. PhD Thesis.
[45] G. Ye, Experimental Study and Numerical Simulation of the Development of the Microstructure and Permeability of Cementitious Materials, PhD Thesis, Delft University of Technology, Delft, The Netherlands, 2003.
[46] Z. Hu, M. Wyrzykowski, K. Scrivener, P. Lura, A novel method to predict internal relative humidity in cementitious materials by 1 H NMR, Cem. Concr. Res. 104 (2018) 80–93.
[47] T. Noguchi, F. Tomosawa, K.M. Nemati, B.M. Chiaia, A.P. Fantilli, A practical equation for elastic modulus of concrete, ACI Struct. J. 106 (2009) 690–696.
[48] H. Chen, M. Wyrzykowski, K. Scrivener, P. Lura, Prediction of self-desiccation in low water-to-cement ratio pastes based on pore structure evolution, Cem. Concr. Res. 49 (2013) 38–47.
[49] V. Baroghel-Bouny, P. Mounanga, A. Khelidj, A. Loukili, N. Rafai, Autogenous deformations of cement pastes: part II. W/C effects, micro-macro correlations, and threshold values, Cem. Concr. Res. 36 (2006) 123–136.
[50] J. Weiss, Experimental determination of the 'time zero', t0 ('Maturity-Zero', M0), in: A. Bentur (Ed.), RILEM Report 25, Early Age Cracking in Cementitious Systems, RILEM Publications S.A.R.L., Cachan, France, 2003, pp. 195–206.
[51] C.W. Miao, Q. Tian, W. Sun, J.P. Liu, Water consumption of the early-age paste and the determination of "time-zero" of self-desiccation shrinkage, Cem. Concr. Res. 37 (2007) 1496–1501.
[52] A. Darquennes, S. Staquet, M. Delplancke-Ogletree, B. Espion, Effect of autogenous deformation on the cracking risk of slag cement concretes, Cem. Concr. Compos. 33 (2011) 368–379.
[53] D.P. Bentz, P.V. Coveney, E.J. Garboczi, M.F. Kleyn, P.E. Stutzman, Cellular automaton simulations of cement hydration and microstructure development, Model. Simul. Mater. Sci. Eng. 2 (1994) 783–808.
[54] S. Bishnoi, K.L. Scrivener, μic: a new platform for modelling the hydration of cements, Cem. Concr. Res. 39 (2009) 266–274.